

# Vertical structure and energetic constraints for a backscatter parameterization of ocean mesoscale eddies

Elizabeth Yankovsky <sup>1</sup>, Scott Bachman <sup>2</sup>, K. Shafer Smith <sup>1</sup>, Laure Zanna <sup>1</sup>

<sup>1</sup>Courant Institute of Mathematical Sciences, New York University, New York, NY

<sup>2</sup>Climate and Global Dynamics Laboratory, National Center for Atmospheric Research, Boulder, CO

## Key Points:

- We propose a parameterization for mesoscale eddies targeting ocean models at eddy-permitting resolutions.
- We find that both the potential and kinetic energy effects of eddies on the flow may be parameterized via a kinetic energy backscatter.
- The novel approach of our backscatter scheme is its use of vertical structure, i.e. backscattering onto the equivalent barotropic mode.

**Abstract**

Mesoscale eddies modulate the stratification, mixing and dissipation pathways, and tracer transport of oceanic flows over a wide range of spatiotemporal scales. The parameterization of buoyancy and momentum fluxes associated with mesoscale eddies thus presents an evolving challenge for ocean modelers, particularly as modern climate models approach eddy-permitting resolutions. Here we present a parameterization targeting such resolutions through the use of a subgrid mesoscale eddy kinetic energy budget (MEKE) framework. Our study presents two novel insights: (1) both the potential and kinetic energy effects of eddies may be parameterized via a kinetic energy backscatter, with no Gent-McWilliams along-isopycnal transport; (2) a dominant factor in ensuring a physically-accurate backscatter is the vertical structure of the parameterized momentum fluxes. We present simulations of  $1/2^\circ$  and  $1/4^\circ$  resolution idealized models with backscatter applied to the equivalent barotropic mode. Remarkably, the global kinetic and potential energies, isopycnal structure, and vertical energy partitioning show significantly improved agreement with a  $1/32^\circ$  reference solution. Our work provides guidance on how to parameterize mesoscale eddy effects in the challenging eddy-permitting regime.

**Plain Language Summary**

Ocean eddies evolving on horizontal lengthscales of order 10-100 km are not sufficiently resolved in modern global ocean models that have horizontal resolutions of about 25-100 km. The under-representation of such eddies leads to inaccuracies in the modelled ocean state, including weakened current systems, incorrect stratification, and erroneous distributions of physical and biological ocean tracers. Here we develop a novel approach to mimicking the unresolved eddy effects by artificially energizing the flow in a way that is consistent with eddy dynamics, specifically their vertical structure. We find that our approach is able to correct for a variety of unresolved eddy effects when employed in a coarse-resolution ocean model and compared against a high-resolution reference case. Our work provides new insights on how to account for unresolved eddies in the next generation of climate models.

**1 Introduction**

As modern ocean models approach horizontal grid resolutions that permit the mesoscale range of motion, modelers face new challenges in developing parameterizations for the incompletely resolved mesoscale eddy dynamics (Griffies et al., 2015; Fox-Kemper et al., 2019; Hewitt et al., 2020). The widely-used Gent and McWilliams (hereafter GM) parameterization mimics the effect of baroclinic instability by adiabatically relaxing large-scale lateral buoyancy gradients (Gent & McWilliams, 1990; Gent et al., 1995). The GM scheme successfully parameterized eddy buoyancy effects in fully non-eddy models but has deleterious effects in eddy-permitting models (Henning & Vallis, 2004; Delworth et al., 2012). Here we define the “eddy-permitting” resolution to be near or below the first baroclinic Rossby deformation scale, with some eddy features captured but being incompletely resolved. Recently, much work has been aimed at parameterizing the momentum effects of eddies through energy “backscatter” schemes (e.g. Kitsios et al. (2013); Jansen and Held (2014); Porta Mana and Zanna (2014); Grooms et al. (2015); Juricke, Danilov, Koldunov, Oliver, Sein, et al. (2020)). Owing to under-resolved dynamics and sub-optimal parameterization choices, ocean models are frequently overly-dissipative — harmonic/biharmonic viscosity removes excess kinetic energy from the flow, and due to the incompletely resolved inverse turbulent cascade, the entire wavenumber spectrum is affected (Juricke, Danilov, Koldunov, Oliver, & Sidorenko, 2020; Khani & Dawson, 2023). The use of GM exacerbates this issue in eddy-permitting models (Hallberg, 2013), by damping the partially-resolved eddies and increasing the kinetic energy deficit. On the contrary, backscatter schemes attempt to correct for the over-dissipation by re-energizing the flow (Jansen et al., 2015).

Backscatter alone may also act to relax APE (Jansen & Held, 2014), further rationalizing its advantage over GM in the eddy-permitting regime.

The premise of parameterizing interactions of the subgrid mesoscale eddy kinetic energy (MEKE) with the resolved flow has gained traction over the last fifteen years (Cessi (2008); Eden and Greatbatch (2008); Marshall and Adcroft (2010), among others). Recently, Jansen et al. (2020) introduced a MEKE-based parameterization framework for ocean models that they argue is scale-aware and suitable for resolutions ranging from non-eddying to eddy-resolving. The premise is to solve a 2D prognostic equation for the MEKE, and use the value of MEKE to inform the GM and backscatter coefficients. The MEKE equation is comprised of source terms from GM and viscous dissipation, sink terms due to backscatter and subgrid dissipation, and a subgrid advective term. A parameterization by Bachman (2019) employs a similar approach, assuming that a fraction of the energy extracted by GM is backscattered to the flow. The argument behind both Bachman (2019) and Jansen et al. (2020) is that the dominant energetic balance represented in the subgrid EKE budget is the eddy-driven extraction of available potential energy (APE) from the mean flow and its conversion into EKE, which experiences the inverse turbulent cascade and is converted into large-scale, resolved kinetic energy.

One of the caveats of using the Jansen et al. (2020) approach arises in an eddy-permitting regime. In this case, GM can have the unfavorable effect of extracting APE from small-scale flow features, such as eddies, rather than the large-scale buoyancy gradients (Mak et al., 2023). Further, backscatter aims to re-energize these features, causing a double-counting of the APE removal. In other words, if an eddy feature is already partially resolved, a preferred parameterization approach would be to energize the eddy so that it can perform the APE extraction from large scales without the need of the GM parameterization. Jansen et al. (2020) propose instead to tune the GM and backscatter components equally. A second caveat lies in the representation of vertical eddy fluxes. The Jansen et al. (2020) scheme uses a 2D, vertically averaged MEKE field for informing the antiviscosity of the backscatter. In situations where the flow is already too baroclinic due to under-resolved eddy vertical fluxes and barotropization, this approach will only maintain or heighten the erroneous vertical structure of the flow.

Here we propose parameterizing mesoscale eddies through kinetic energy backscatter without the use of GM in an effort to avoid the aforementioned negative effects of GM at eddy-permitting resolutions. We will show that both the kinetic and potential energy effects of unresolved mesoscale eddies on the resolved flow may be parameterized by a correctly formulated backscatter term. The key component maintaining energetic consistency in our backscatter parameterization is imposing an equivalent barotropic vertical structure onto the backscatter antiviscosity, computed using a 2D MEKE budget. Although a fully 3D MEKE budget has been explored by Juricke et al. (2019); Juricke, Danilov, Koldunov, Oliver, and Sidorenko (2020), we choose to avoid the additional degrees of freedom in parameterizing inter-layer fluxes, computational expense, and implementation challenges, and retain a 2D budget. Instead, we will incorporate a 3D structure into the backscatter antiviscosity based on the equivalent barotropic dynamical mode that is representative of EKE vertical structure (de La Lama et al., 2016). In this study we will be employing the idealized model NeverWorld2 (Marques et al., 2022) as a testbed for developing our backscatter scheme. The paper will begin by providing details of the NeverWorld2 configuration and the parameterization formulation. We will then compare the results of a high-resolution ( $1/32^\circ$ ) reference simulation, an unparameterized low-resolution ( $1/2^\circ$ ) simulation, a  $1/2^\circ$  simulation with our backscatter scheme, and a  $1/2^\circ$  simulation using the Jansen et al. (2020) approach of equally tuned GM and backscatter. Various metrics related to the buoyancy and energetic structure of the simulations will be compared to assess the performance of our backscatter scheme. We will then discuss limitations and new questions that the scheme raises and end with conclusions.

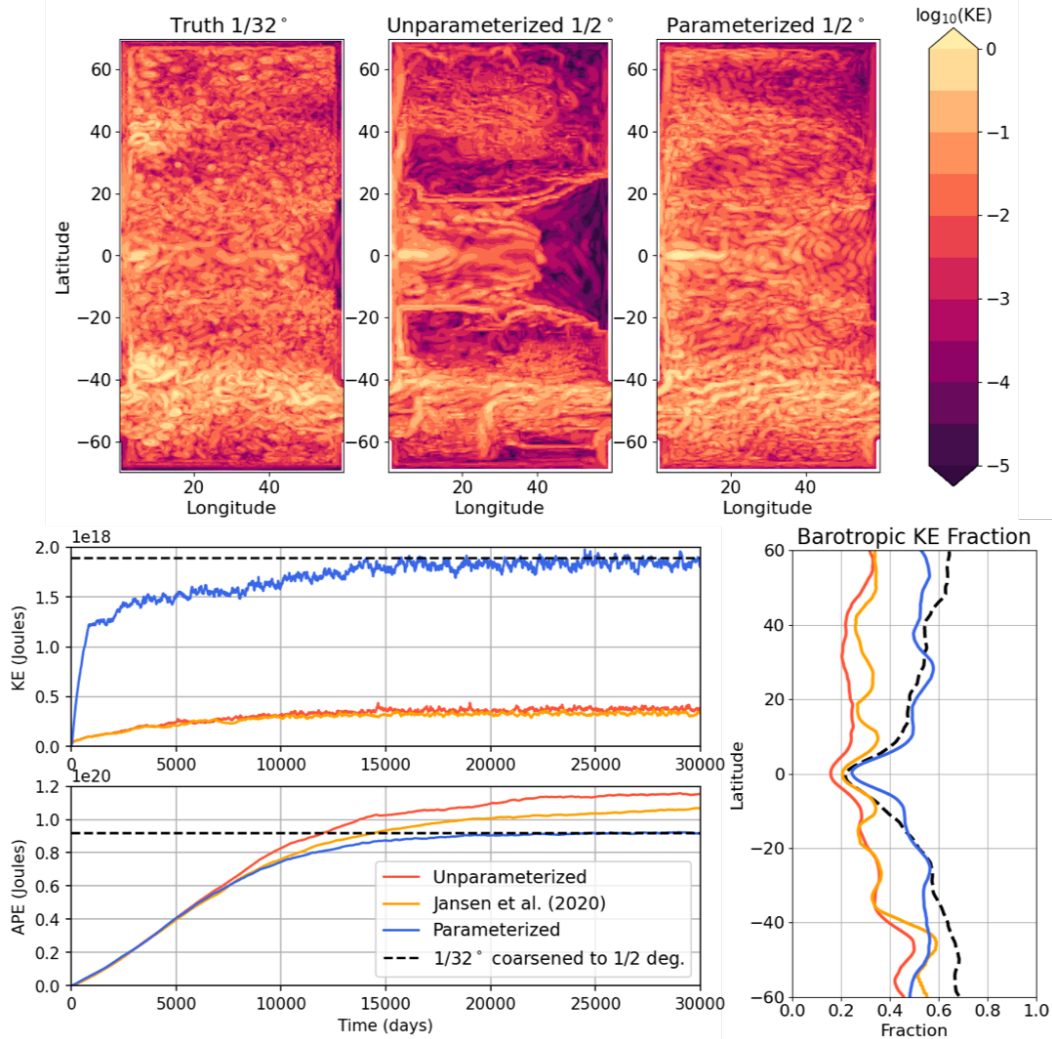


**Figure 1.** Upper row: 5-day averaged surface kinetic energy on a logarithmic scale for a high-resolution ( $1/32^\circ$ ) reference simulation, a low-resolution ( $1/2^\circ$ ) simulation with no eddy parameterization, and a low-resolution ( $1/2^\circ$ ) simulation with our backscatter scheme. The  $1/2^\circ$  simulation using the Jansen et al. (2020) scheme looks nearly identical to the unparameterized case when considering the surface KE (not shown). Lower left: timeseries of globally integrated kinetic and available potential energy for the  $1/2^\circ$  unparameterized case, the Jansen et al. (2020) and our backscatter parameterizations, and the reference simulation’s steady-state values coarsened onto a  $1/2^\circ$  grid. Lower right: zonally-averaged values of the fraction of kinetic energy in the barotropic mode of the flow for the same simulations.

## 2 A testbed for eddy parameterization development

To develop and validate our parameterization, we have employed the NeverWorld2 (NW2) model detailed in Marques et al. (2022). NW2 is an adiabatic, stacked shallow water configuration of the GFDL-MOM6. It represents a two-hemisphere idealization of the Atlantic Ocean, with a topographic ridge extending through the middle of the domain and a channel representing the Southern Ocean in the southern hemisphere. The model is forced only by a meridionally-varying, temporally constant wind. As such, the model provides a well-tailored means by which to study and parameterize ocean eddies driven by baroclinic instability, whose physics are predominantly adiabatic.

Prior works (e.g., Kjellsson and Zanna (2017) in a realistic global model, Yankovsky et al. (2022) in the idealized NW2), have considered how the representation of mesoscale eddies changes as a function of resolution and what effects under-resolved eddies have on the resolved flow. A main finding of these studies is that the vertical structure of the flow becomes increasingly baroclinic as the model resolution is coarsened. The vertical eddy energy fluxes that lead to barotropization (Smith & Vallis, 2001; Chemke & Kaspi, 2016) are not fully captured at eddy-permitting resolutions. Additionally, as resolution is coarsened the APE of the flow becomes higher and the KE lower. We hypothesize that these issues may be mediated by the use of a backscatter with vertical structure representing that of EKE in a high-resolution model.

In Marques et al. (2022) and Yankovsky et al. (2022) we considered a hierarchy of four horizontal resolutions of NW2:  $1/4^\circ$ ,  $1/8^\circ$ ,  $1/16^\circ$ , and  $1/32^\circ$ . The  $1/32^\circ$  was taken as the “truth” and lower resolutions were compared against it. The most fundamental shift in flow properties occurred between the  $1/4^\circ$  and  $1/8^\circ$  resolutions. The  $1/8^\circ$  and higher resolution models all had similar vertical flow structure; the main difference was the kinetic energy of the flow. By contrast, at  $1/4^\circ$  the baroclinic Rossby radius is unresolved over most of the domain and the flow vertical structure is significantly more baroclinic than the higher resolutions. Although eddies are present and grid spacing is close to the deformation radius, the inverse energy cascade driven by eddies is unresolved. A study by Loose et al. (2022) also considered scale-dependent energetics in the NW2 model as a basis for developing scale- and flow-aware parameterizations particularly for eddy-permitting models. For NW2 (and ocean models more broadly), we consider the eddy-permitting resolution to begin roughly at  $1/2^\circ$  to  $1/4^\circ$ . We will thus focus on the  $1/2^\circ$  case – the more challenging limit as it is barely eddy-permitting – when developing and testing our parameterization.

We will discuss the details of our parameterization below, but we begin with a demonstration of our scheme’s performance. Figure 1 shows an overview of how our parameterization compares against the Jansen et al. (2020) scheme and an unparameterized simulation at  $1/2^\circ$  resolution as well as the high-resolution “truth” case ( $1/32^\circ$ ). The surface KE in the truth case shows a richly eddying structure throughout the domain. The highest energies are seen in the Southern Ocean, where wind stress is largest, as well as in the western boundary current region in the northern hemisphere. The unparameterized  $1/2^\circ$  simulation is significantly less energetic, noting that the figure uses a logarithmic color scale. There are zones where the energy is nearly three orders of magnitude smaller than the truth case, such as in the midlatitudes, eastern low latitudes, and northernmost part of the domain. Additionally, due to the constant-in-time wind forcing and lack of resolved eddies, there are unphysical zonal bands of high energy. The  $1/2^\circ$  simulation using the Jansen et al. (2020) scheme (not shown in the upper panel) looks nearly identical to the unparameterized case when considering the surface KE distribution. In our parameterized  $1/2^\circ$  simulation, we see a remarkable improvement in the surface energy levels and structure. The zonal features arising in the unparameterized case are no longer evident and the energy levels are comparable to that of the truth case. The Southern Ocean and western boundary current regions also have better resemblance with the truth case. The globally integrated kinetic and potential energy for the same three cases and the Jansen et al. (2020) case are shown in the bottom of Figure 1. The  $1/2^\circ$  case with our parameterization has a global APE and

KE that is nearly identical to that of the truth case coarsened onto a  $1/2^\circ$  grid, whereas the unparameterized case has overly high APE and a KE nearly an order of magnitude smaller. The Jansen et al. (2020) case has roughly the correct APE but the KE is nearly the same as the unparameterized case. Finally, the vertical structure of the flow with our parameterization on is substantially improved relative to the unparameterized and Jansen et al. (2020) cases. We see a much larger portion of the KE in the barotropic part of the flow, in line with the truth case.

### 3 Parameterization formulation

The momentum equation of the resolved flow is

$$\partial_t \mathbf{u} + (f + \zeta) \hat{\mathbf{z}} \times \mathbf{u} + \nabla(K + M) = \frac{1}{\rho_0} \frac{\partial \boldsymbol{\tau}}{\partial z} - \nabla \cdot [\nu_4 \nabla(\nabla^2 \mathbf{u})] + \nabla \cdot (\nu_2 \nabla \mathbf{u}). \quad (1)$$

Here,  $\mathbf{u} = (u, v)$  is the horizontal velocity vector,  $f = 2\Omega \sin \theta$  is the Coriolis parameter (with  $\Omega = 7.2921 \times 10^{-5} \text{ s}^{-1}$  and latitude  $\theta$ ),  $\zeta = \partial_x v - \partial_y u$  is relative vorticity,  $\hat{\mathbf{z}}$  is the unit vector in the vertical direction, and  $\nabla = (\partial_x, \partial_y)$  is the horizontal gradient. The kinetic energy density is  $K$ , Montgomery potential is  $M$ , and  $\boldsymbol{\tau}$  is vertical stress. The second-to-last term is biharmonic dissipation, where  $\nu_4$  is set using the Smagorinsky scheme (Griffies & Hallberg, 2000),

$$\nu_4 = (c_{\text{smag}} |\sqrt{(\partial_x u - \partial_y v)^2 + (\partial_y u + \partial_x v)^2}|) \Delta^4, \quad (2)$$

with  $c_{\text{smag}} = 0.2$  (Marques et al., 2022) and  $\Delta$  is horizontal grid spacing. The last term in (1) is an antiviscous harmonic backscatter, and the form of its coefficient,  $\nu_2$ , shapes the eddy parameterization. In most of the results presented here, we set

$$\nu_2 = c\sqrt{2e}L_{\text{mix}}, \quad (3)$$

where  $c$  is a nondimensional tuning parameter that is negative for backscatter,  $L_{\text{mix}}$  is the subgrid-scale mixing length (set as the minimum of the grid spacing and the generalized Rhines scale, following Jansen et al. (2020)), and  $e = e(x, y, t)$  is vertically-averaged subgrid Mesoscale Eddy Kinetic Energy (MEKE).

Subgrid MEKE is set using a local dynamic budget proposed by Jansen et al. (2020),

$$\partial_t e = \dot{e}_{\text{GM}} + \dot{e}_{\text{Smag}} - \dot{e}_{\text{BScat}} - \dot{e}_{\text{diss}} - \dot{e}_{\text{adv}}. \quad (4)$$

There are two source terms of subgrid EKE. The first is  $\dot{e}_{\text{GM}}$ , determined by the rate at which a GM parameterization (if used) converts potential energy (PE) from the resolved flow to EKE through buoyancy diffusion. The second is  $\dot{e}_{\text{Smag}}$ , capturing the rate at which biharmonic Smagorinsky viscosity extracts KE from the resolved flow. The sinks of subgrid EKE are  $\dot{e}_{\text{BScat}}$ , the backscatter of EKE into the resolved flow implemented via the harmonic antiviscosity term, and  $\dot{e}_{\text{diss}}$ , the subgrid frictional dissipation of EKE in the bottom boundary layer, parameterized using a quadratic drag law. The last term in (4) is the horizontal transport of subgrid EKE parameterized via diffusion and advection by the resolved barotropic flow, and should integrate to zero over the domain. For further details see Jansen et al. (2020).

A novel component of the parameterization presented here is the imposition of vertical structure in the antiviscous coefficient, so that  $\nu_2 = \nu_2(z)$ . Through a great deal of experimentation, we found that to improve the fidelity of parameterized simulations, two aspects of its vertical structure were particularly important: its amplitude should be surface-intensified, and vanish at the ocean's floor. This is consistent with an analysis of moored current meters by de La Lama et al. (2016), showing that the ocean's kinetic energy projects strongly onto the Equivalent Barotropic Mode (EBT), and further buttressed by theoretical arguments that this is consistent with the effects of rough bottom topography on EKE (LaCasce, 2017). We leverage this result in our parameterization; although we do

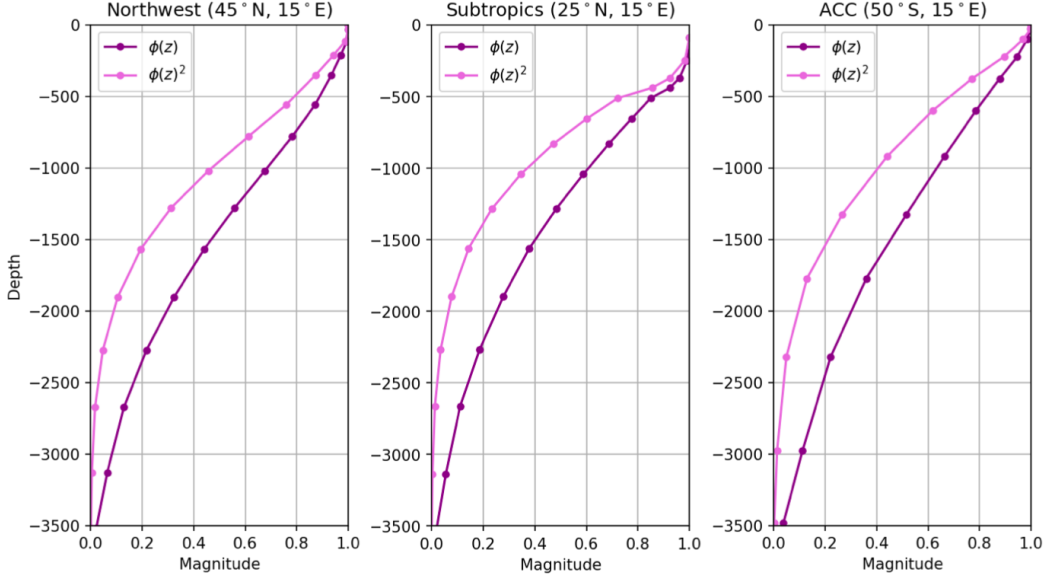


**Figure 2.** EBT mode structure at three locations within the NW2 domain – Northwest, subtropics, and Antarctic Circumpolar Current. The EBT mode as derived above is for the horizontal velocity structure; we additionally plot the square of the EBT mode to reflect the vertical structure of the kinetic energy. Note that the above EBT mode structures were computed for a coarse-resolution  $1/2^\circ$  NW2 configuration (consistent with the higher resolution cases, not shown).

not explicitly resolve the vertical energy fluxes driven by ocean eddies, we parameterize the expected end state in which the EKE has a vertical structure that is well-approximated by the EBT mode.

The EBT mode arises from the eigenvector problem for the quasigeostrophic stretching operator,

$$\frac{d}{dz} \left( \frac{f^2}{N^2} \frac{d\phi_j}{dz} \right) + \lambda_j^2 \phi_j = 0. \quad (5)$$

Here  $f$  is the Coriolis parameter,  $N(z)$  is the buoyancy frequency,  $\phi_j(z)$  are the eigenvectors, and  $\lambda_j^2$  are the associated eigenvalues, with  $j = 0, 1, 2, \dots$ . The traditional baroclinic modes are the eigenvectors that arise with Neumann boundary conditions at the surface and bottom, i.e.  $d\phi/dz = 0$  at  $z = 0, -H$ . In this case  $\lambda_0 = 0$ , and  $\phi_0(z) = 1$  is the standard barotropic mode, equivalent to a depth-average. If one instead uses a Neumann condition at the top and a Dirichlet condition at the bottom, i.e.

$$\left. \frac{d\phi}{dz} \right|_{z=0} = 0 \quad \text{and} \quad \phi|_{z=-H} = 0, \quad (6)$$

one finds that the first eigenvalue  $\lambda_0 \neq 0$ , and the first eigenvector  $\phi_0(z)$  is depth-dependent, with a surface-intensified structure and a vanishing amplitude at the bottom;  $\phi_0(z)$  is the EBT mode, hereafter denoted simply  $\phi(z)$ .

We obtain the EBT mode’s vertical structure by numerically solving (5) using the local buoyancy frequency with rigid lid surface and Dirichlet bottom boundary conditions. The resulting  $\phi(z)$  is plotted for three sample locations in Figure 3. Assuming  $\phi(z)$  reflects the structure of eddy horizontal velocity, then its square, also shown, corresponds to the vertical structure of EKE. In most of the results that follow, we set the backscatter antiscatter coefficient as

$$\nu_2 = \phi(z)^2 c \sqrt{2e} L_{\text{mix}}. \quad (7)$$

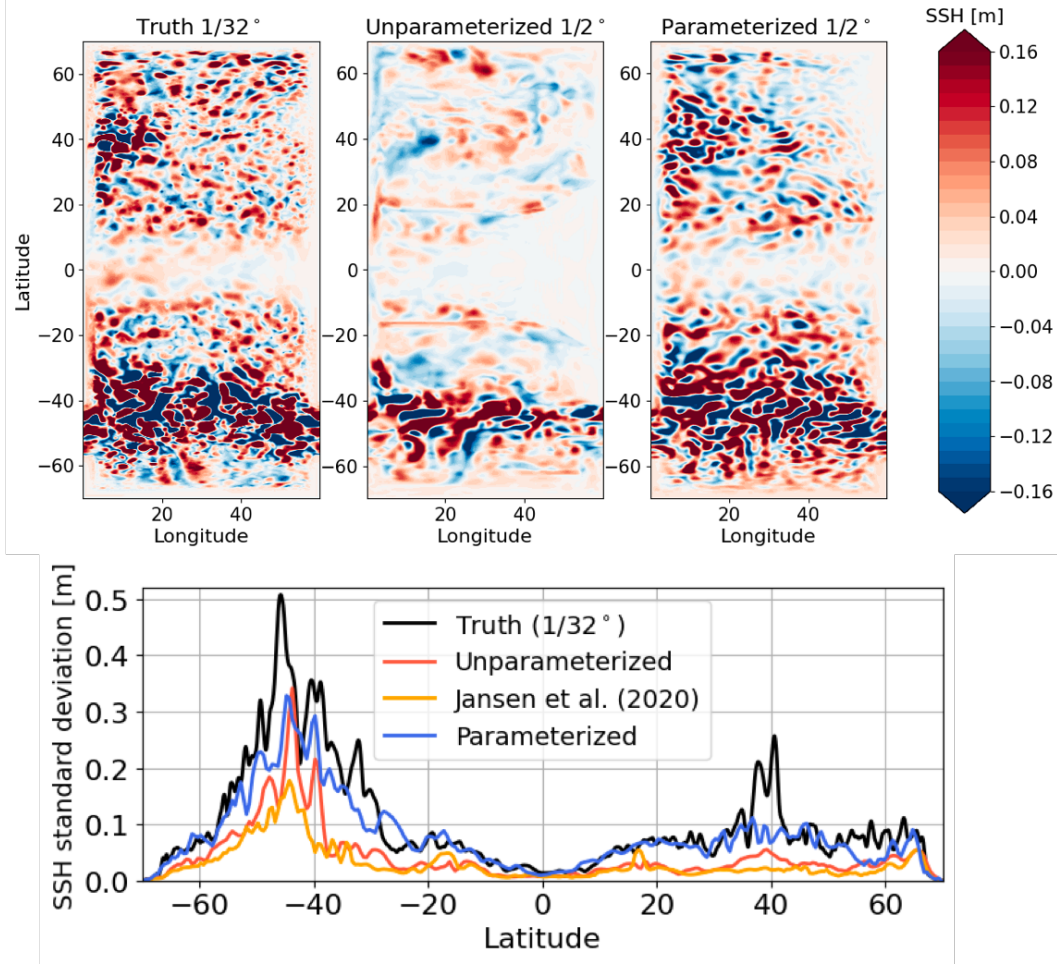


**Figure 3.** Upper row: 5-day averaged sea surface height anomaly relative to a 500-day climatology for the reference ( $1/32^\circ$ ) simulation,  $1/2^\circ$  simulation with no eddy parameterization, and  $1/2^\circ$  simulation with our backscatter scheme turned on. Lower row: zonally averaged standard deviation of SSH computed for a 5-day averaged field for the same simulations and the Jansen et al. (2020)  $1/2^\circ$  case.

Alternative formulations for  $\nu_2$  are considered in Section 5.

The final novel component of our scheme is the use of a technique to stabilize the backscatter. The premise of using a biharmonic operator to dissipate energy and a harmonic (Laplacian) operator to backscatter energy is to attempt to return energy to the flow at larger scales than it is being removed (Jansen & Held, 2014). In practice, however, this approach can lead to numerical instability. In some instances,  $\dot{e}_{\text{BScat}}$  can locally inject energy faster than  $\dot{e}_{\text{Smag}}$ ,  $\dot{e}_{\text{adv}}$ , and  $\dot{e}_{\text{diss}}$  can remove it. We have therefore formulated a criterion for avoiding such instability by implementing a backscatter shutoff when the dissipation term  $\dot{e}_{\text{Smag}}$  reaches a threshold value. This technique is described in greater detail in Section 5. For further details on the terms of the MEKE budget, see Jansen et al. (2020) and references therein. For further details on the numerics of our scheme and an alternative formulation for the antivitycosity see Section 5 and the appendix.

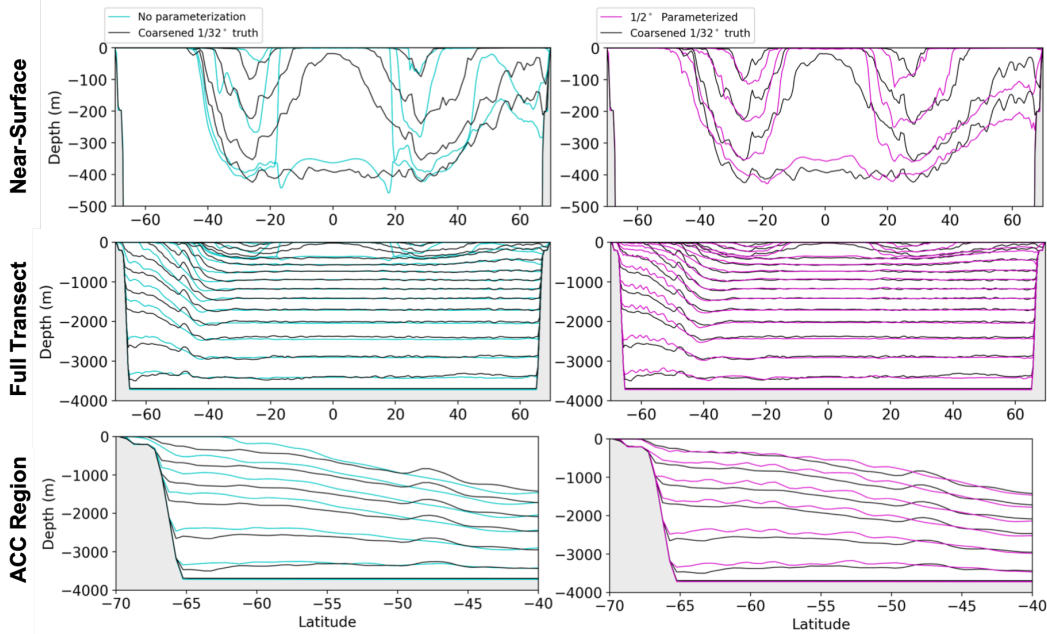


**Figure 4.** Left column: 500-day averaged isopycnal positions through  $45^\circ$  longitude for the  $1/2^\circ$  simulation with no eddy parameterization. Right column: same, for  $1/2^\circ$  simulation with our backscatter scheme. Top row is the upper 5 isopycnals, middle row shows all isopycnals, and lowest row shows lowest 6 isopycnals in the Southern Ocean. In all plots, black lines show the coarsened reference ( $1/32^\circ$ ) simulation’s isopycnal positions.

#### 4 Evaluating our parameterization

We now evaluate a suite of metrics for a  $1/2^\circ$  simulation with and without our parameterization turned on. The metrics will be compared against a  $1/32^\circ$  reference solution. For some metrics we will additionally show the results from a  $1/2^\circ$  simulation employing the Jansen et al. (2020) scheme in its default configuration with GM and backscatter active. As observed in Figure 1, the global APE and KE of the parameterized case is consistent with the reference case. We next ask whether local properties over the model domain are similarly consistent. In Figure 3 we consider the field of the sea surface height (SSH) anomaly, where one may observe the eddy field. The truth and parameterized simulations show similar variability and structure across latitudes. The unparameterized case has markedly less variability, particularly in the meridional direction and in regions where the flow is less energetic. The standard deviation of SSH as a function of latitude also shows good agreement between the parameterized and truth cases. The Jansen et al. (2020) case, by contrast, has even less variability than the unparameterized case – emphasizing the problem of eddy-damping by GM and the inability of the backscatter to compensate. Thus, our backscatter scheme appears to be energizing eddies with appropriate scale and structure across latitudes.

We next consider the density structure as a function of latitude. In Figure 4, meridional transects of 500-day averaged isopycnal positions are compared between the unparameterized, parameterized, and truth cases. The unparameterized case has overly steep isopycnals at all levels (less obvious in the quiescent abyssal ocean). The locations of the isopycnal outcrops in the Southern Ocean are erroneous compared to the truth case. In the case with our parameterization, the isopycnals are much closer to the reference solution. However, there are still regions in which there are differences with the truth case, such as very low latitudes where eddy dynamics become less pronounced. Although this result has been seen

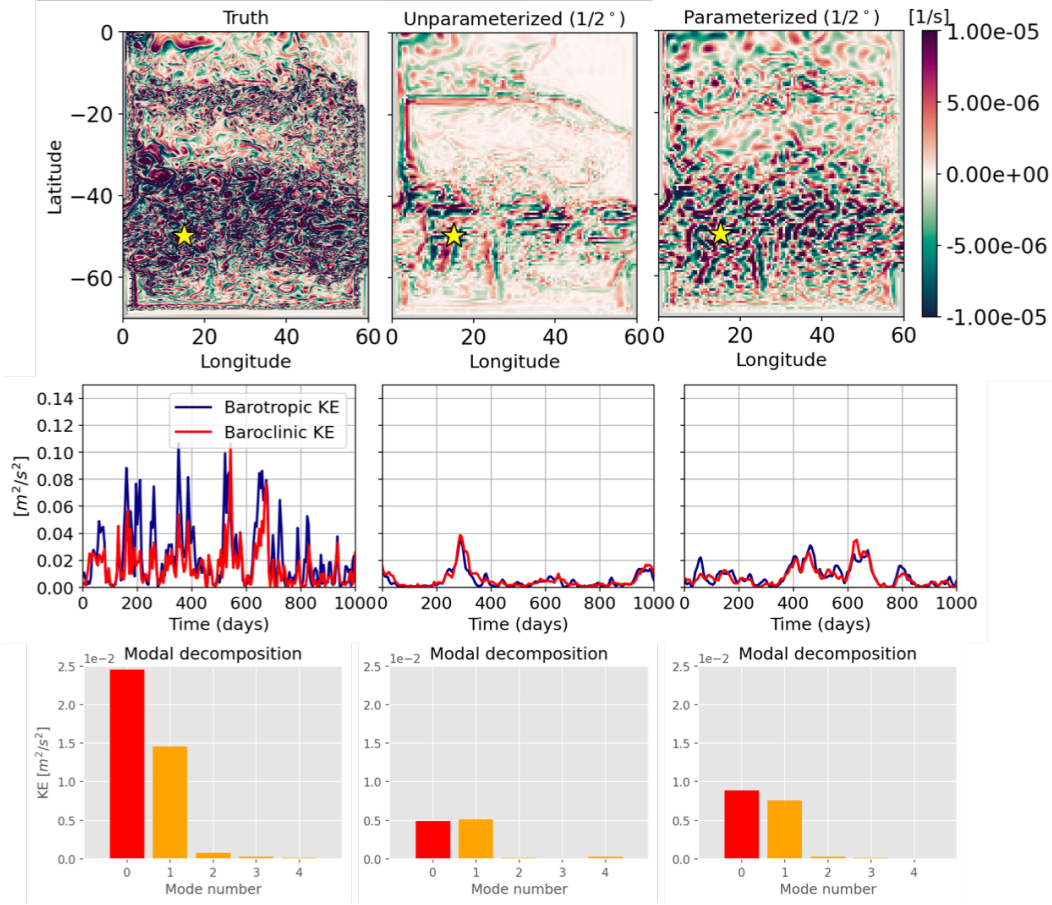


**Figure 5.** Left to right columns: Southern Ocean in the reference ( $1/32^\circ$ ) simulation,  $1/2^\circ$  case with no eddy parameterization,  $1/2^\circ$  case with our backscatter scheme. Top to bottom: 5-day averaged surface vorticity field, barotropic and baroclinic kinetic energy timeseries, and 500-day averaged decomposition of kinetic energy by vertical mode. The zeroth mode refers to the barotropic mode. In the latter two panels, we consider the starred point in the upper panel.

in simulations with GM, such as Jansen et al. (2020), here we parameterize the buoyancy effects of eddies by using a kinetic energy backscatter alone. By energizing existing eddies in the flow in a physical manner, we are able to allow them to perform the extraction of APE from the large-scale flow without the need for an additional GM-like buoyancy closure at this resolution.

We next consider the kinetic energy structure of the flow in greater detail. As shown in Yankovsky et al. (2022), one of the hallmarks of under-resolved eddies is energy trapping in the baroclinic vertical modes of the flow. Figures 5-6 consider two locations (northern hemisphere and the Southern Ocean, respectively). The vorticity fields at both locations are significantly improved between the case without/with our parameterization turned on (relative to the  $1/32^\circ$  case). We decompose the kinetic energy into its baroclinic and barotropic constituents and plot them as time series; again the case with our parameterization is mostly in line with the reference case. Finally we consider the modal decomposition of the kinetic energy, by computing the vertical modes of the flow assuming flat bottom boundary conditions and plotting the kinetic energy associated with each vertical mode. As expected, the unparameterized case has a dominant energy component in the baroclinic part of the flow due to the unresolved vertical eddy fluxes and barotropization process. In the truth and

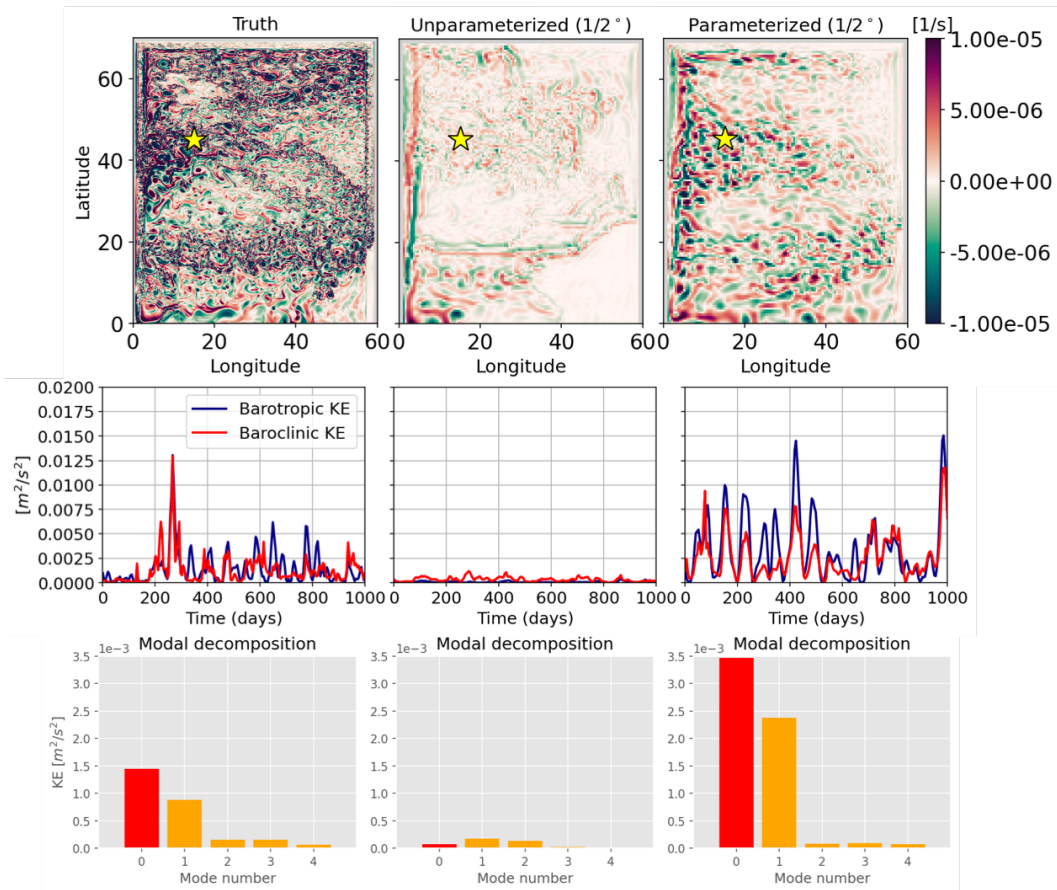


**Figure 6.** Same as in Figure 5, but for the northern hemisphere.

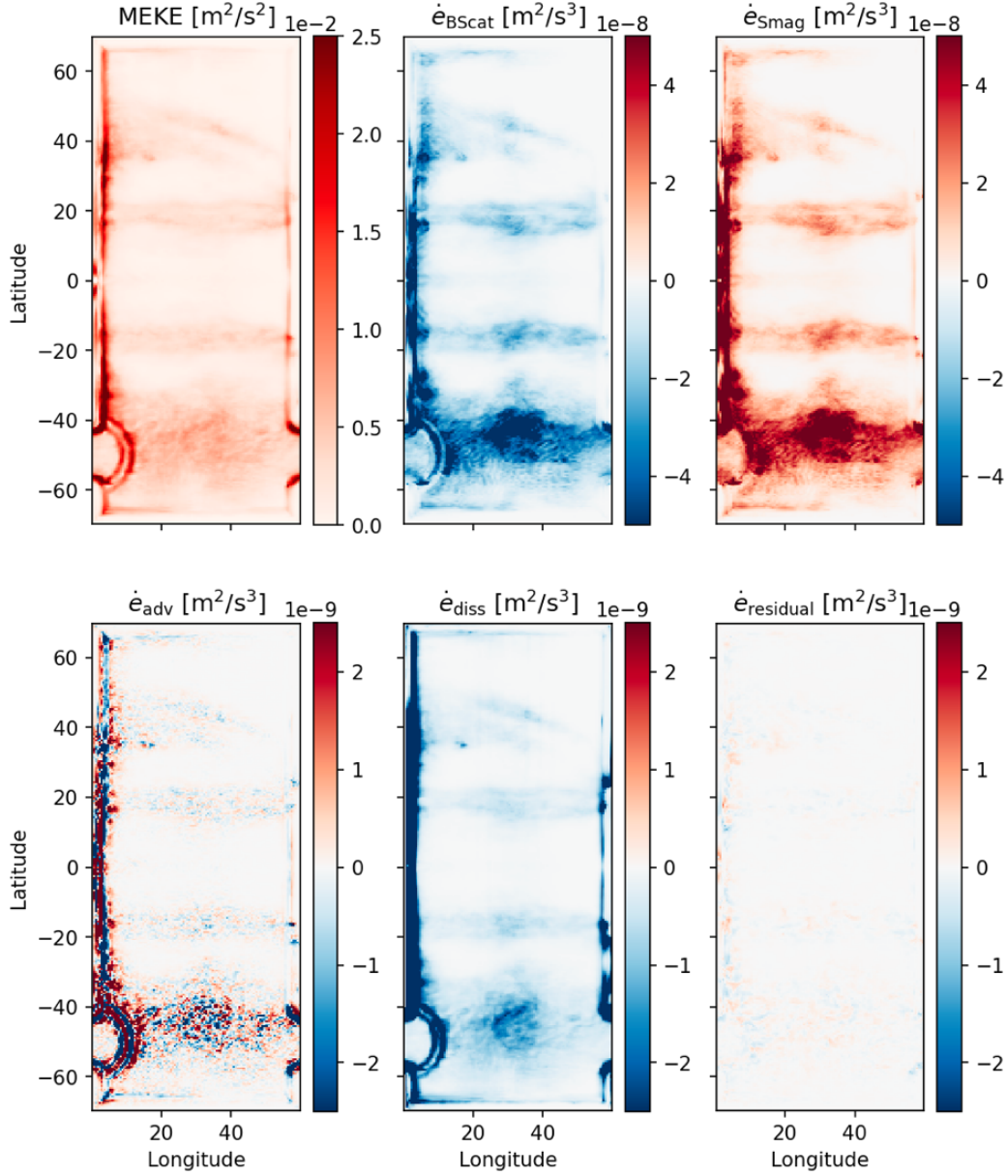


**Figure 7.** Subgrid mesoscale eddy kinetic energy (MEKE) computed from the MEKE budget and averaged over 500 days for the 1/2° case with our backscatter scheme (upper left), terms and residual of the MEKE budget (other panels). Note that the Smagorinsky and backscatter terms are dominant, and have a colorbar scale 20 times that of the other terms.

parameterized case we see a dominant part of the kinetic energy in the barotropic part of the flow (there are some discrepancies due to the fact that this is a pointwise measurement). These results may be compared against an analogous analysis for various configurations of the Jansen et al. (2020) scheme in Figure 9; in the latter the problem of under-barotropized and under-energized flow persists. We thus find that our parameterization is representing the unresolved eddy influences on vertical structure in an appropriate way.

To gain a better understanding of the subgrid MEKE budget (4), we consider planview plots of the constituent terms in Figure 7. We observe the highest subgrid MEKE values to be occurring in regions where the eddy activity is most vigorous and wind forcing is the highest, particularly the western boundary current region and Southern Ocean. The subgrid MEKE terms are primarily a balance between the backscatter and the biharmonic dissipation (the former is a sink of MEKE, the latter a source). The subgrid advection and frictional effects play a secondary role in the parameterization, being roughly an order of magnitude smaller.

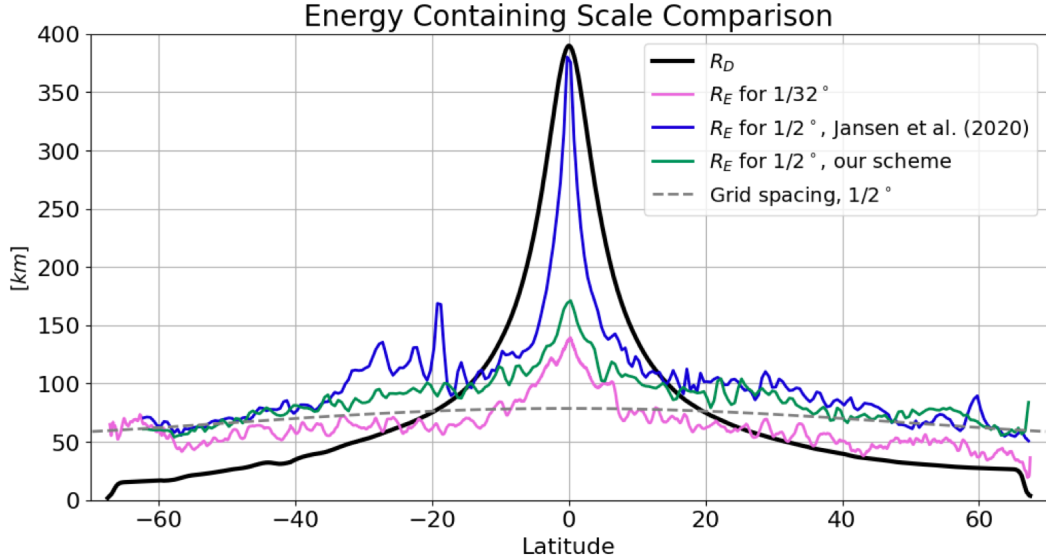


**Figure 8.** Zonally and 500-day averaged deformation scale (for  $1/32^\circ$  case) and energy-containing scale for the  $1/32^\circ$  case,  $1/2^\circ$  case with the Jansen et al. (2020) scheme, and our  $1/2^\circ$  backscatter case. Grid spacing for the  $1/2^\circ$  simulations is shown in dashed grey.

As an additional metric to assess the performance of our parameterization, we are interested in considering whether the eddies we energize through the kinetic energy backscatter are of a physical scale. We compute the energy-containing scale  $R_E$  (interpreted as the eddy scale) according to Thompson and Young (2006) using the field of the sea surface height anomaly ( $\eta'_0$ ) relative to a 500-day climatology as:

$$R_E = \sqrt{\frac{\langle \eta_0'^2 \rangle}{\langle |\nabla \eta_0'|^2 \rangle}}, \quad (8)$$

where angle brackets denote time averaging over 500 days. In Figure 8 we compare  $R_E$  between the truth ( $1/32^\circ$ ), a  $1/2^\circ$  case with the Jansen et al. (2020) scheme turned on, and a  $1/2^\circ$  with our backscatter parameterization. For reference, the deformation scale is shown in black and the grid spacing in dashed grey. We see that the energy-containing scale for the case with our parameterization is relatively close to that of the truth case, and lies slightly above the grid scale. This contrasts with the Jansen et al. (2020) case, where the

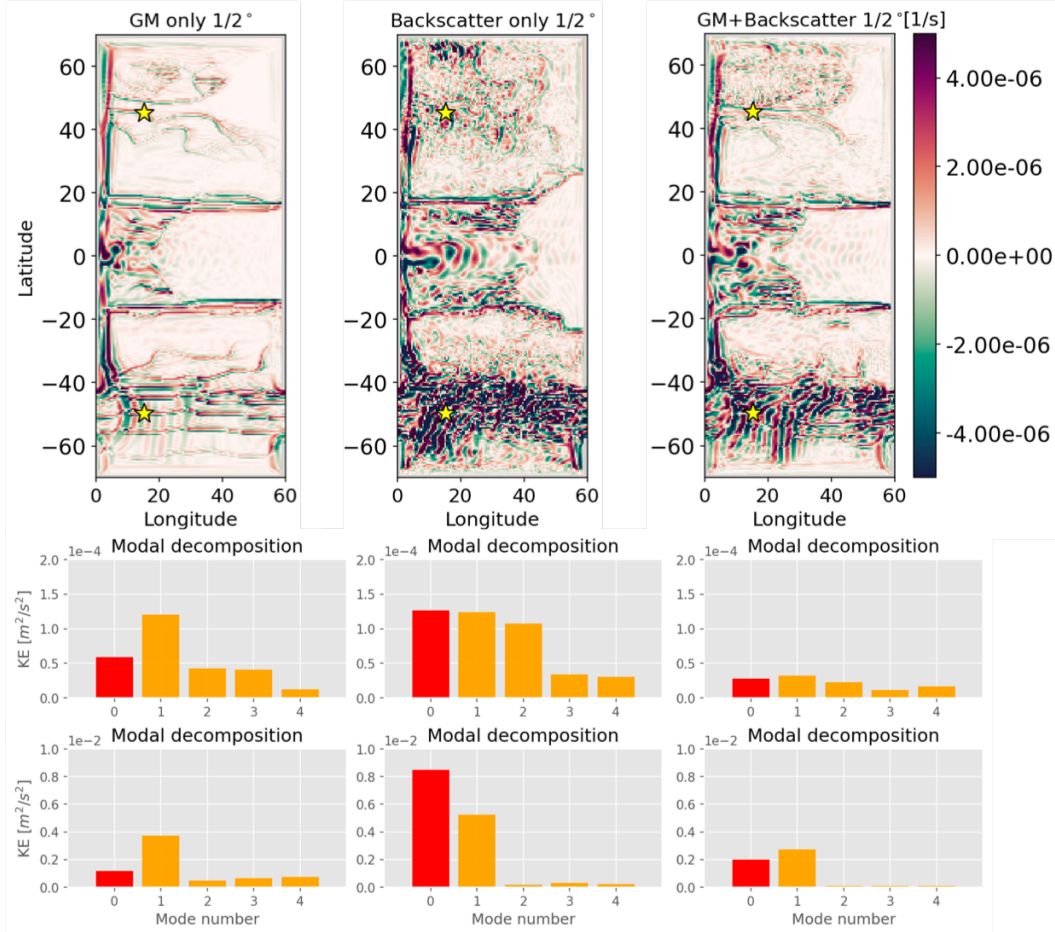


**Figure 9.** Comparison of 5-day averaged surface vorticity (top panel), and 500-day averaged kinetic energy decomposition into vertical modes (as in Figures 5, 6) for the two starred locations shown in the top panel. Middle row is for the northern location and lower row is for the southern location. The left column uses only the Gent-McWilliams component of the Jansen et al. (2020) scheme, middle uses only the backscatter component of Jansen et al. (2020), and right uses the default Jansen et al. (2020) setup with both GM and backscatter with equal tuning coefficients.

energy scale is significantly larger than the reference simulation. This result further adds validity to our backscatter approach – the eddies are growing to a reasonable size, following a physical dissipation pathway that arrests their growth.

## 5 Discussion

Having shown that our backscatter scheme produces significant improvements to the flow state relative to an unparameterized case at  $1/2^\circ$ , we now provide more discussion on how our scheme offers advantages to prior parameterization approaches and discuss its development process. We began the development of this scheme by testing both the Bachman (2019) and Jansen et al. (2020) schemes in the NW2 model. In particular, we were interested in how to tune the GM and backscatter components for an eddy-permitting model. We first asked: should we tune the GM and backscatter components with the same tuning constant (as suggested by Jansen et al. (2020))? Is it advantageous to rely more on GM, more on backscatter, or a combination of the two? In Figure 9 we examine the

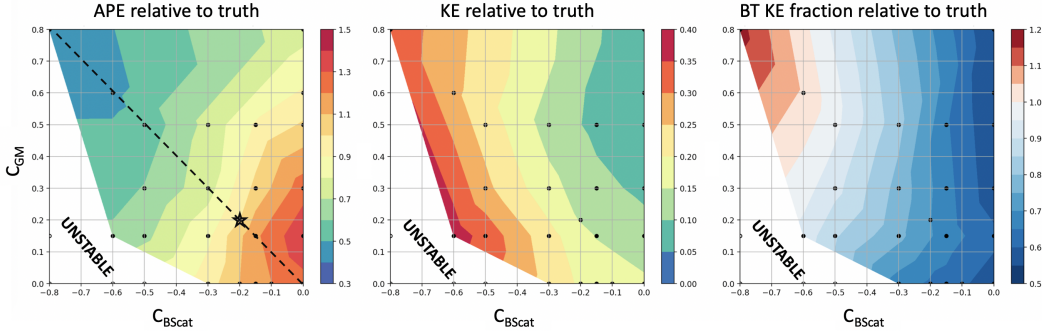


**Figure 10.** Here we consider three metrics – globally integrated available potential energy (APE) and kinetic energy (KE), as well as globally averaged barotropic KE fraction. The metrics are computed for a suite of  $1/2^\circ$  simulations using the Jansen et al. (2020) scheme, varying the tuning coefficient before the Gent-McWilliams ( $c_{GM}$ ) and backscatter ( $c_{BS}$ ) terms. They are then divided by the value of the same metric for the reference  $1/32^\circ$  simulation coarsened onto a  $1/2^\circ$  grid, so that a value of 1.0 represents a simulation that is in line with the reference solution.

surface vorticity and decomposition of KE into vertical modes for simulations using the Jansen et al. (2020) scheme with GM only, backscatter only, and equally tuned GM and backscatter. Although none of the simulations have the correct vertical energy partitioning with barotropization accurately captured, we see the most resemblance in the vorticity field of the backscatter only case when compared against the reference solution (Figure 5-6).

To further guide the scaling of GM vs. backscatter at the eddy-permitting regime, we considered a parameter sweep across variable GM and backscatter tuning constants (Figure 10). We computed the global APE, KE, and average barotropic KE component of the coarsened reference simulation and compared it against  $1/2^\circ$  simulations with varying GM and backscatter coefficients. We found that by all metrics, the backscatter only case performed the best – the KE, APE, and vertical structure are dominantly set by the backscatter coefficient, not GM magnitude. However, for high values of backscatter the simulation becomes unstable. This motivated us to explore methods to stabilize the backscatter and turn off GM for eddy-permitting resolutions.

Figure 11 summarizes our hypothesis for what causes the backscatter to become numerically unstable. As shown in Figure 7, the dominant energy balance in the subgrid EKE budget is between the backscatter sink and viscous source terms. The same two terms are present in the momentum equation of the resolved flow as an antiscalability and viscosity (respectively). In some instances, an eddy feature having high subgrid EKE and thus a high backscatter amplitude falls into a feedback cycle where the backscatter and dissipation both grow in magnitude. The viscous dissipation is unable to remove energy as quickly as it is being put in by the backscatter and the velocities within the eddy feature become extreme, leading to numerical instability. As a result, we circumvent this feedback loop by implementing a backscatter shutoff based on a viscous CFL criterion. Within the GFDL-MOM6 there is a CFL limit on how large the biharmonic viscosity  $\nu_4$  may be (given by  $\Delta^4/dt$ , where  $\Delta$  is grid spacing and  $dt$  is time step). When  $\nu_4$  reaches 1/4 of this limit, we modify the subgrid EKE budget by removing the viscous source term and shutting off backscatter:

$$\partial_t e = -\dot{e}_{\text{diss}} - \dot{e}_{\text{adv}}. \quad (9)$$

The use of a value of 1/4 is somewhat empirical, we found this value to be restrictive enough to prevent numerical instability but not too restrictive in turning off the backscatter.

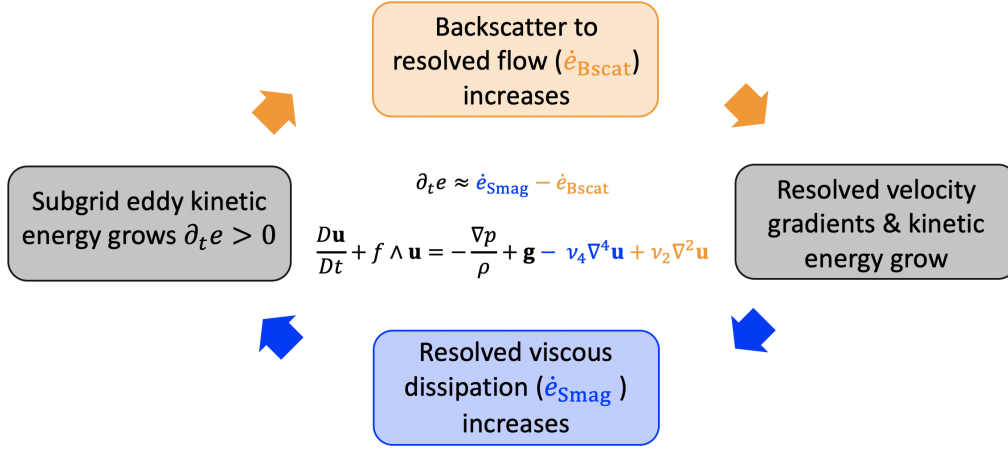


**Figure 11.** Diagram showing the feedback loop that can lead to instability in the backscatter parameterization. The feedback occurs when the backscatter (having a harmonic operator) and viscous dissipation prescribed in the model (here a Smagorinsky scheme with a biharmonic operator) have little scale separation in a particular region of the flow or eddy feature. The two operators act on the same region, causing a rapid increase in energy and extreme velocities; the CFL condition is violated and the model blows up.

Another question we were interested in exploring is whether the functional form of the antiviscosity affects the performance of the parameterization. We began with the Jansen et al. (2020) form of the antiviscosity (Equation 3) and multiplied this by the squared equivalent barotropic vertical structure (Equation 7). The idea behind this scaling is a mixing length argument – the eddy velocity scale is related to the square root of the subgrid EKE and the mixing length refers to the eddy arrest scale. We tested a second approach which has a different scaling for the antiviscosity  $\nu_2(z)$ , but retains the same EBT vertical structure. The alternative scaling has the form:

$$\nu_2(z) = c \frac{2e}{\|\dot{\mathbf{s}}\|} \phi^4(z), \quad (10)$$

where  $\dot{\mathbf{s}}$  is the strain rate tensor and  $\|\cdot\|$  is the tensor norm operator. This approach is based on deriving the theoretical upper bound on the antiviscosity (see Appendix A for the derivation). This scaling has a linear relationship between the eddy energy and antiviscosity. The linear relationship between eddy energy and diffusivity, where viscosity may be thought of as a momentum diffusivity, has its origins in the approach used in the GEOMETRIC mesoscale eddy parameterization (Marshall et al., 2012; Mak et al., 2018, 2022). For consistency with Equation 7 we raise the power of the EBT mode to 4, since we found that the power of 2 best represents the vertical structure of the square root of the EKE. Remarkably, we found that the two approaches produce nearly identical results. Figure 12 shows the timeseries of globally integrated KE and APE for the two scaling choices – they appear to overlap and agree with the high-resolution reference simulation. This further emphasizes that the crucial piece of the backscatter parameterization is having a decaying vertical structure. For reference, the figure also shows the Jansen et al. (2020) approach using both backscatter and GM with no vertical structure, although the APE is somewhat close to the reference solution, the KE is almost an order of magnitude smaller than in our two backscatter simulations.

To further study the role of the vertical structure in the backscatter, we tested several other choices for modulating  $\nu_2$  by a vertical structure (not shown in the figures). We first hypothesized that the best way to parameterize eddy vertical structure effects would be to

consider the “final” part of the turbulent energy cascade – the inverse cascade of energy in the barotropic mode. We implemented a barotropic version of the backscatter and tuned it such that the global KE matched that of the reference simulation. Interestingly, the APE of this simulation was significantly too low. We also tested a first baroclinic modal structure (using flat bottom modes); again due to the nonzero magnitude near the bottom we found that too much APE was being removed from the flow. We switched to a constant decay scale with depth (testing values of 500 and 700 meters), which significantly improved the solution and motivated us to try the EBT mode (which similarly decays to a zero value near the bottom). This proved to be an appropriate choice; when we tuned this case so that the KE matched that of the truth case, the APE also perfectly matched.

Finally, to test the scale awareness of our parameterization within the eddy-permitting regime, we additionally ran a suite of NW2 simulations at  $1/4^\circ$ , with different tuning coefficient values. The timeseries of KE and APE for these simulations is shown in Figure 13. Based on the fact that a tuning coefficient of  $-1.0$  was used at  $1/2^\circ$ , one would expect that at this doubled resolution the correct tuning coefficient would be around  $-0.5$ . Indeed, we see that when  $c = -0.5$ , the KE matches with the coarsened high-resolution result. The APE is also very close to the reference, although slightly low. This brings up another interesting point – the scale awareness of the vertical structure. Based on experiments testing various formulations of vertical structure, we find that an overly low APE (for the correct KE structure) occurs when the vertical structure does not decay sufficiently rapidly with depth, i.e. the barotropic component is overly large. This means that at  $1/4^\circ$ , to have a better agreement with the APE of the reference simulation, we should make the backscatter slightly more surface-intensified. To this end, recent work by Zhang et al. (2023) suggests the possibility that a different modal structure, such as the surface quasi-geostrophic mode, may be used in place of the EBT mode.

## 6 Conclusions

We have presented a mesoscale eddy parameterization formulated as a momentum closure incorporating vertical structure into the parameterized fluxes. The parameterization relies on the mesoscale eddy kinetic energy (MEKE) budget framework, where a prognostic equation for eddy energy informs the backscatter magnitude. The backscatter is applied onto the equivalent barotropic (EBT) mode, which has a maximum near the surface and decays to zero near the bottom. Our scheme is aimed at representing both kinetic energy and potential energy influences of mesoscale eddies in the challenging eddy-permitting regime through the sole use of backscatter. We have tested the parameterization in the idealized NeverWorld2 model, at  $1/2^\circ$  and  $1/4^\circ$  resolutions. The results of the parameterized runs show that applying the backscatter to the EBT mode results in global kinetic and potential energies, isopycnal structure, and vertical energy partitioning that are consistent with a  $1/32^\circ$  reference simulation. By energizing the EBT mode we attempt to artificially mimic the end state of the eddy fluxes and interactions that give rise to an EBT vertical structure. Note that our backscatter scheme maintains the approach of using a 2D vertically averaged MEKE field, as in Jansen et al. (2015), unlike the approach proposed by Eden and Greatbatch (2008) and Juricke et al. (2019) of using a 3D EKE field. The 2D approach, while being computationally less expensive, also bypasses the need to represent vertical eddy fluxes between layers, for which there is limited theoretical guidance.

An important aspect of our parameterization that requires some additional work is its scale awareness, and in particular how the scheme should be implemented in a realistic climate model that may range from eddy-permitting to non-eddying in various parts of the globe. As we emphasized in the introduction, our scheme specifically targets eddy-permitting resolutions where eddy features are already present in the flow; the objective is to reinforce them in a physical manner through backscatter rather than damping them through GM. The approach employed by Jansen et al. (2020) was to use a resolution function (as proposed by Hallberg (2013), but smooth rather than step-like in form) dependent on

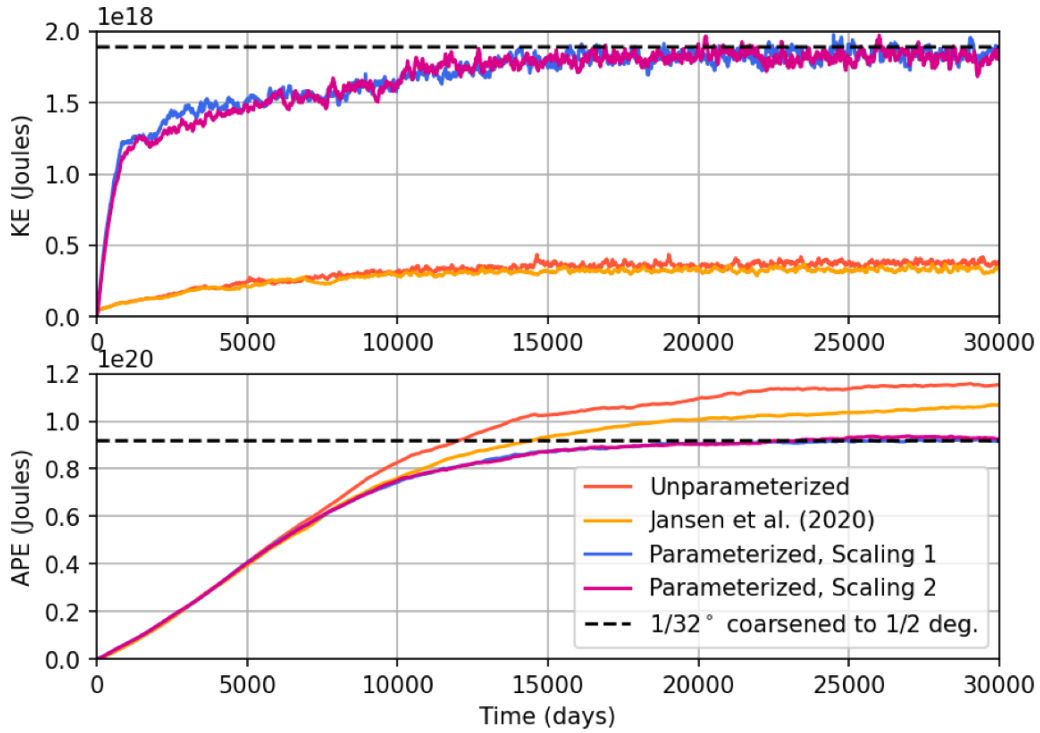


**Figure 12.** Timeseries of globally integrated kinetic and available potential energy for several  $1/2^\circ$  simulations and the reference ( $1/32^\circ$ ) simulation’s steady-state values coarsened onto a  $1/2^\circ$  grid. Red is the unparameterized case, orange is the tuned Jansen et al. (2020) parameterization, and blue and violet lines are our backscatter approach with two scalings. Scaling 1 uses the Jansen et al. (2020) approach to solve for the antiscalability amplitude (then modifying it by the equivalent barotropic mode structure), whereas scaling 2 uses a linear dependence between the subgrid eddy kinetic energy and the antiscalability (also modifying by the equivalent barotropic mode). We see that the form of the antiscalability does not matter nearly as much for the flow energetics as the inclusion of vertical structure.

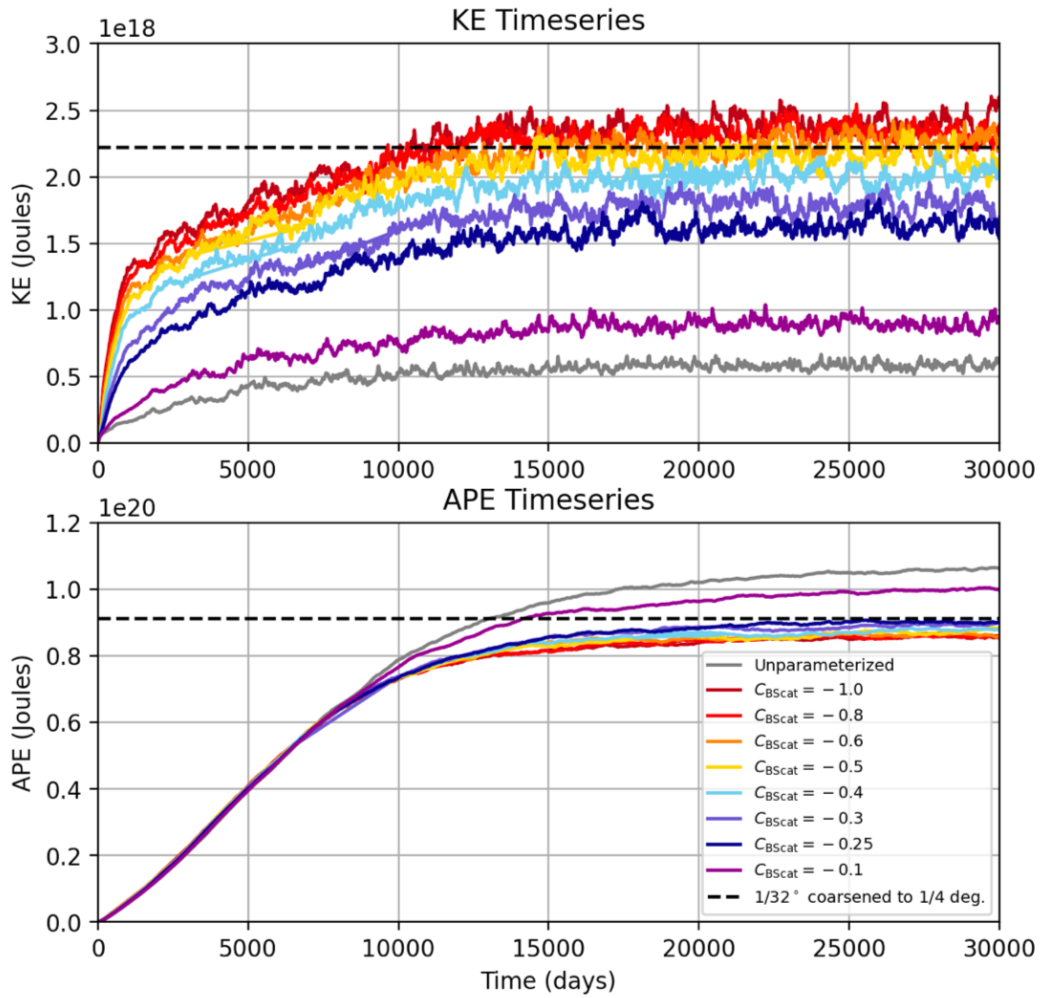


**Figure 13.** Timeseries of globally integrated kinetic and available potential energy for  $1/4^\circ$  simulations using our backscatter scheme, varying the tuning coefficient magnitude from 0.1 to 1.0. Also shown is the reference ( $1/32^\circ$ ) simulation's steady-state values coarsened onto a  $1/4^\circ$  grid.

the deformation radius  $R_D$  as a scaling factor to mediate the backscatter and GM terms of the MEKE budget (Equation 4). When  $R_D$  is resolved, both the backscatter and GM terms are scaled to zero; when unresolved, they are scaled with equal magnitudes.

Based on our results, the scale-awareness approach of Jansen et al. (2020) does not appear to be the optimal choice. At coarse resolutions where eddies are not resolved, we suggest that backscatter be turned off entirely while GM serves as the dominant parameterization of eddy buoyancy effects. As the resolution increases and eddying features are increasingly permitted, backscatter magnitude should increase whereas GM should be diminished. At these resolutions GM damps the eddies that backscatter attempts to energize, and leads to double-counting of the APE removal – as we saw, properly energizing the partially-resolved eddies leads to APE removal without GM. Further, backscatter may yield beneficial results even when resolutions are around/just above the deformation scale. Thus, having an identical resolution function and coefficients for the GM and backscatter components is not recommended based on our results. Although developing the proper resolution function for backscatter and GM across all model resolutions is beyond the scope of this paper, we do encourage increased reliance on backscatter rather than GM at horizontal model resolutions of order  $R_D$  and finer. Another avenue for future research that we did not consider in this study is how to approach isoneutral diffusion (Redi, 1982; Griffies et al., 1998).

This research provides valuable guidance for ocean modelers on how to parameterize mesoscale eddy effects in eddy-permitting regimes. The study opens new questions in how to best scale backscatter vs. the Gent-McWilliams eddy parameterization component to ensure scale-awareness across all model resolutions. We also hope to build upon efforts of implementing backscatter in realistic ocean models (Chang et al., 2023) and investigate in greater depth how our parameterization performs in a fully coupled climate model.

## Appendix A Bounding the viscous coefficient using eddy energy

Here we derive a theoretical upper bound for the backscatter antiviscosity, which we test as an alternative formulation to the Jansen et al. (2020) scaling in Section 5. The energy tendency of the viscous operator is given by

$$\mathcal{D} = \frac{1}{2} \boldsymbol{\sigma} : \dot{\mathbf{s}}, \quad (\text{A1})$$

where under Reynolds averaging

$$\boldsymbol{\sigma} = \begin{bmatrix} \overline{u'u'} & \overline{u'v'} \\ \overline{u'v'} & \overline{v'v'} \end{bmatrix} \quad (\text{A2})$$

is the Reynolds stress tensor and

$$\dot{\mathbf{s}} = \begin{bmatrix} \overline{u_x} & \frac{1}{2}(\overline{v_x} + \overline{u_y}) \\ \frac{1}{2}(\overline{v_x} + \overline{u_y}) & \overline{v_y} \end{bmatrix} \quad (\text{A3})$$

is the strain rate tensor. Bars indicate time-averaged quantities and primes represent fluctuations. We will employ a standard harmonic eddy viscosity parameterization of the form

$$\boldsymbol{\sigma} = \mathbf{A} : \dot{\mathbf{s}}, \quad (\text{A4})$$

where  $\mathbf{A}$  is a fourth-order tensor satisfying the usual symmetries (e.g. Smith and McWilliams, 2003). We will assume a scalar viscosity, in which case (A4) reduces to

$$\boldsymbol{\sigma} = \nu \dot{\mathbf{s}}. \quad (\text{A5})$$

We seek to bound the magnitude of the coefficient  $\nu$ . We start by employing the Cauchy-Schwartz inequality,

$$|\langle \boldsymbol{\sigma}, \dot{\mathbf{s}} \rangle| \leq \| \boldsymbol{\sigma} \| \| \dot{\mathbf{s}} \|, \quad (\text{A6})$$

where  $\langle \cdot \rangle$  is the Frobenius/matrix inner product and  $\|\cdot\|$  is the Frobenius norm. Substituting (A5) into (A6), this becomes

$$|\langle \nu \dot{\mathbf{s}}, \dot{\mathbf{s}} \rangle| = |\nu| \|\dot{\mathbf{s}}\|^2 \quad (\text{A7})$$

$$\leq \|\boldsymbol{\sigma}\| \|\dot{\mathbf{s}}\|, \quad (\text{A8})$$

and so

$$|\nu| \leq \frac{\|\boldsymbol{\sigma}\|}{\|\dot{\mathbf{s}}\|}. \quad (\text{A9})$$

We now seek a bound for  $\|\boldsymbol{\sigma}\|$ . By the definition of the Frobenius norm, we have

$$\|\boldsymbol{\sigma}\| = \left( \overline{u'^2} + 2\overline{u'v'^2} + \overline{v'^2} \right)^{1/2}, \quad (\text{A10})$$

and by Hölder's inequality we have

$$\left( \int_S u'v' dx \right)^2 \leq \left( \int_S u'^2 dx \right) \left( \int_S v'^2 dx \right) \quad (\text{A11})$$

for some measurable subset  $S$  of  $\mathbb{R}^n$ , so if we define our averaging operator to be  $\overline{(\cdot)} = \int_S (\cdot) dx$  we have

$$\overline{u'v'^2} \leq \overline{u'^2} \overline{v'^2}. \quad (\text{A12})$$

Defining the eddy kinetic energy  $e = \frac{1}{2}(\overline{u'^2} + \overline{v'^2})$ , we can substitute (A12) into (A10) to obtain the bound

$$\|\boldsymbol{\sigma}\| \leq (4K^2)^{1/2} = 2e. \quad (\text{A13})$$

Finally, we can substitute (A13) back into (A9) to obtain the final bound,

$$|\nu| \leq \frac{2e}{\|\dot{\mathbf{s}}\|} \quad (\text{A14})$$

$$= \frac{2e}{\left( \overline{u_x^2} + \frac{1}{2}(\overline{v_x} + \overline{u_y})^2 + \overline{v_y^2} \right)^{1/2}} \quad (\text{A15})$$

Note that this bound applies for both positive and negative  $\nu$ , meaning it can be used to constrain both dissipation and backscatter coefficients.

## Open Research

The Jupyter notebooks used to generate figures in the manuscript are available in a Zenodo repository at <https://doi.org/10.5281/zenodo.8350252>. We also include configuration files and 500 days of data for three  $1/2^\circ$  simulations presented in this manuscript – the case with no parameterization, the Jansen et al. (2020) scheme, and our new parameterization (see Sections 2, 4). The NeverWorld2 configuration used in this manuscript is detailed in Marques et al. (2022). The MOM6 source code and NeverWorld2 configuration files are available at <https://doi.org/10.5281/zenodo.6993951> (Bhamidipati et al., 2022). The NeverWorld2 dataset and detailed information on its contents are available at <https://doi.org/10.26024/f130-ev71> (Marques, 2022).

## Acknowledgments

The authors thank the members of the Ocean Transport and Eddy Energy Climate Process Team for insightful discussions, advice, and support throughout the course of this project. EY, KSS, and LZ were supported by NSF grant OCE 1912357 and NOAA CVP NA19OAR4310364. SB was supported by NSF grant OCE 1912420.

## References

- Bachman, S. D. (2019). The GM+E closure: A framework for coupling backscatter with the Gent and McWilliams parameterization. *Ocean Modelling*, *136*, 85–106. doi: 10.1016/j.ocemod.2019.02.006
- Bhamidipati, N., Adcroft, A., Marques, G., & Abernathey, R. (2022, April). *ocean-eddy-cpt/NeverWorld2: NeverWorld2-description-paper*. Zenodo [code]. doi: 10.5281/zenodo.6462289
- Cessi, P. (2008). An energy-constrained parameterization of eddy buoyancy flux. *Journal of Physical Oceanography*, *38*(8), 1807–1819. doi: 10.1175/2007JPO3812.1
- Chang, C.-Y., Adcroft, A., Zanna, L., Hallberg, R., & Griffies, S. M. (2023). Remote versus local impacts of energy backscatter on the North Atlantic SST biases in a global ocean model. *In prep. for Geophysical Research Letters*.
- Chemke, R., & Kaspi, Y. (2016). The latitudinal dependence of the oceanic barotropic eddy kinetic energy and macroturbulence energy transport. *Geophysical Research Letters*, *43*(6), 2723–2731. doi: 10.1002/2016GL067847
- de La Lama, M. S., LaCasce, J. H., & Fuhr, H. K. (2016). The vertical structure of ocean eddies. *Dynamics and Statistics of the Climate System*, *1*(1). doi: 10.1093/climsys/dzw001
- Delworth, T. L., Rosati, A., Anderson, W., Adcroft, A. J., Balaji, V., Benson, R., ... Zhang, R. (2012). Simulated climate and climate change in the GFDL CM2.5 high-resolution coupled climate model. *Journal of Climate*, *25*(8), 2755–2781. doi: 10.1175/JCLI-D-11-00316.1
- Eden, C., & Greatbatch, R. J. (2008). Towards a mesoscale eddy closure. *Ocean Modelling*, *20*(3), 223–239. doi: 10.1016/j.ocemod.2007.09.002
- Fox-Kemper, B., Adcroft, A., Böning, C. W., Chassignet, E. P., Curchitser, E., Danabasoglu, G., ... Yeager, S. G. (2019). Challenges and prospects in ocean circulation models. *Frontiers in Marine Science*, *6*.
- Gent, P. R., & McWilliams, J. C. (1990). Isopycnal mixing in ocean circulation models. *Journal of Physical Oceanography*, *20*(1), 150–155. doi: 10.1175/1520-0485(1990)020<0150:IMIOCM>2.0.CO;2
- Gent, P. R., Willebrand, J., McDougall, T. J., & McWilliams, J. C. (1995). Parameterizing eddy-induced tracer transports in ocean circulation models. *Journal of Physical Oceanography*, *25*(4), 463–474. doi: 10.1175/1520-0485(1995)025<0463:PEITTI>2.0.CO;2
- Griffies, S. M., Gnanadesikan, A., Pacanowski, R. C., Larichev, V. D., Dukowicz, J. K., & Smith, R. D. (1998). Isonutral diffusion in a z-coordinate ocean model. *Journal of Physical Oceanography*, *28*(5), 805–830. doi: 10.1175/1520-0485(1998)028<0805:IDIAZC>2.0.CO;2
- Griffies, S. M., & Hallberg, R. W. (2000). Biharmonic friction with a Smagorinsky-like viscosity for use in large-scale eddy-permitting ocean models. *Monthly Weather Review*, *128*(8), 2935–2946. doi: 10.1175/1520-0493(2000)128<2935:BFWASL>2.0.CO;2
- Griffies, S. M., Winton, M., Anderson, W. G., Benson, R., Delworth, T. L., Dufour, C. O., ... Zhang, R. (2015). Impacts on ocean heat from transient mesoscale eddies in a hierarchy of climate models. *Journal of Climate*, *28*(3), 952–977. doi: 10.1175/JCLI-D-14-00353.1
- Grooms, I., Majda, A. J., & Smith, K. S. (2015). Stochastic superparameterization in a quasigeostrophic model of the Antarctic Circumpolar Current. *Ocean Modelling*, *85*, 1–15. doi: 10.1016/j.ocemod.2014.10.001
- Hallberg, R. (2013). Using a resolution function to regulate parameterizations of oceanic mesoscale eddy effects. *Ocean Modelling*, *72*, 92–103. doi: 10.1016/j.ocemod.2013.08.007
- Henning, C. C., & Vallis, G. K. (2004). The effects of mesoscale eddies on the main subtropical thermocline. *Journal of Physical Oceanography*, *34*(11), 2428–2443. doi: 10.1175/JPO2639.1

- Hewitt, H. T., Roberts, M., Mathiot, P., Biastoch, A., Blockley, E., Chassignet, E. P., ... Zhang, Q. (2020). Resolving and parameterising the ocean mesoscale in earth system models. *Current Climate Change Reports*, 6(4), 137–152. doi: 10.1007/s40641-020-00164-w
- Jansen, M. F., Adcroft, A., Khani, S., & Kong, H. (2020). Toward an energetically consistent, resolution aware parameterization of ocean mesoscale eddies. *Journal of Advances in Modeling Earth Systems*, 11(8), 2844–2860. doi: <https://doi.org/10.1029/2019MS001750>
- Jansen, M. F., & Held, I. M. (2014). Parameterizing subgrid-scale eddy effects using energetically consistent backscatter. *Ocean Modelling*, 80, 36–48. doi: 10.1016/j.ocemod.2014.06.002
- Jansen, M. F., Held, I. M., Adcroft, A., & Hallberg, R. (2015). Energy budget-based backscatter in an eddy permitting primitive equation model. *Ocean Modelling*, 94. doi: 10.1016/j.ocemod.2015.07.015
- Juricke, S., Danilov, S., Koldunov, N., Oliver, M., Sein, D., Sidorenko, D., & Wang, Q. (2020). A kinematic kinetic energy backscatter parametrization: From implementation to global ocean simulations. *Journal of Advances in Modeling Earth Systems*, 12. doi: 10.1029/2020MS002175
- Juricke, S., Danilov, S., Koldunov, N., Oliver, M., & Sidorenko, D. (2020). Ocean kinetic energy backscatter parametrization on unstructured grids: impact on global eddy-permitting simulations. *Journal of Advances in Modeling Earth Systems*, 12(1). doi: 10.1029/2019MS001855
- Juricke, S., Danilov, S., Kutsenko, A., & Oliver, M. (2019). Ocean kinetic energy backscatter parametrizations on unstructured grids: Impact on mesoscale turbulence in a channel. *Ocean Modelling*, 138, 51–67. doi: 10.1016/j.ocemod.2019.03.009
- Khani, S., & Dawson, C. N. (2023). A gradient based subgrid-scale parameterization for ocean mesoscale eddies. *Journal of Advances in Modeling Earth Systems*, 15(2). doi: 10.1029/2022MS003356
- Kitsios, V., Frederiksen, J. S., & Zidikheri, M. J. (2013). Scaling laws for parameterisations of subgrid eddy–eddy interactions in simulations of oceanic circulations. *Ocean Modelling*, 68, 88–105. doi: 10.1016/j.ocemod.2013.05.001
- Kjellsson, J., & Zanna, L. (2017). The impact of horizontal resolution on energy transfers in global ocean models. *Fluids*, 2(3), 45. doi: 10.3390/fluids2030045
- LaCasce, J. H. (2017). The prevalence of oceanic surface modes. *Geophysical Research Letters*, 44(21), 11,097–11,105. doi: 10.1002/2017GL075430
- Loose, N., Bachman, S., Grooms, I., & Jansen, M. (2022). Diagnosing scale-dependent energy cycles in a high-resolution isopycnal ocean model. *Journal of Physical Oceanography*, 53(1), 157–176. doi: 10.1175/JPO-D-22-0083.1
- Mak, J., Maddison, J., Marshall, D., Ruan, X., Wang, Y., & Yeow, L. (2023). Scale-awareness in an eddy energy constrained mesoscale eddy parameterization. *Journal of Advances in Modeling Earth Systems*. doi: 10.48550/arXiv.2306.08988
- Mak, J., Maddison, J. R., Marshall, D. P., & Munday, D. R. (2018). Implementation of a geometrically informed and energetically constrained mesoscale eddy parameterization in an ocean circulation model. *Journal of Physical Oceanography*, 48(10), 2363–2382. doi: 10.1175/JPO-D-18-0017.1
- Mak, J., Marshall, D. P., Madec, G., & Maddison, J. R. (2022). Acute sensitivity of global ocean circulation and heat content to eddy energy dissipation timescale. *Geophysical Research Letters*, 49(8), e2021GL097259. doi: 10.1029/2021GL097259
- Marques, G. (2022). *NeverWorld2 [Dataset]*. UCAR/NCAR - CISL - CDP. (Type: dataset) doi: 10.26024/F130-EV71
- Marques, G., Loose, N., Yankovsky, E., Steinberg, J. M., Chang, C.-Y., Bhamidipati, N., ... Zanna, L. (2022). NeverWorld2: an idealized model hierarchy to investigate ocean mesoscale eddies across resolutions. *Geoscientific Model Development*, 15(17), 6567–6579. doi: 10.5194/gmd-15-6567-2022
- Marshall, D. P., & Adcroft, A. J. (2010). Parameterization of ocean eddies: Potential

- vorticity mixing, energetics and Arnold's first stability theorem. *Ocean Modelling*, 32(3), 188–204. doi: 10.1016/j.ocemod.2010.02.001
- Marshall, D. P., Maddison, J. R., & Berloff, P. S. (2012). A framework for parameterizing eddy potential vorticity fluxes. *Journal of Physical Oceanography*, 42(4), 539–557. doi: 10.1175/JPO-D-11-048.1
- Porta Mana, P., & Zanna, L. (2014). Toward a stochastic parameterization of ocean mesoscale eddies. *Ocean Modelling*, 79, 1–20. doi: 10.1016/j.ocemod.2014.04.002
- Redi, M. H. (1982). Oceanic isopycnal mixing by coordinate rotation. *Journal of Physical Oceanography*, 12(10), 1154–1158. doi: 10.1175/1520-0485(1982)012<1154:OIMBCR>2.0.CO;2
- Smith, K. S., & Vallis, G. K. (2001, February). The scales and equilibration of midocean eddies: Freely evolving flow. *Journal of Physical Oceanography*, 31(2), 554–571. doi: 10.1175/1520-0485(2001)031<0554:TSAEOM>2.0.CO;2
- Thompson, A. F., & Young, W. R. (2006). Scaling baroclinic eddy fluxes: vortices and energy balance. *Journal of Physical Oceanography*, 36(4), 720–738. doi: 10.1175/JPO2874.1
- Yankovsky, E., Zanna, L., & Smith, K. S. (2022). Influences of mesoscale ocean eddies on flow vertical structure in a resolution-based model hierarchy. *Journal of Advances in Modeling Earth Systems*, 14(11), e2022MS003203. doi: 10.1029/2022MS003203
- Zhang, W., Griffies, S., Hallberg, R., & Wolfe, C. L. P. (2023). The role of surface PV in the vertical structure of mesoscale eddies. *In prep. for Journal of Physical Oceanography*.

Figure 2.

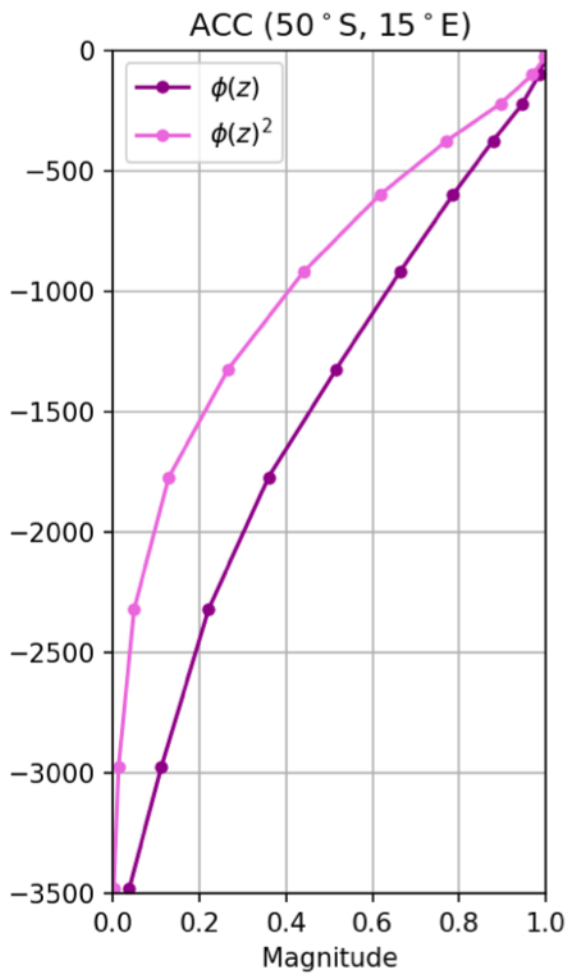
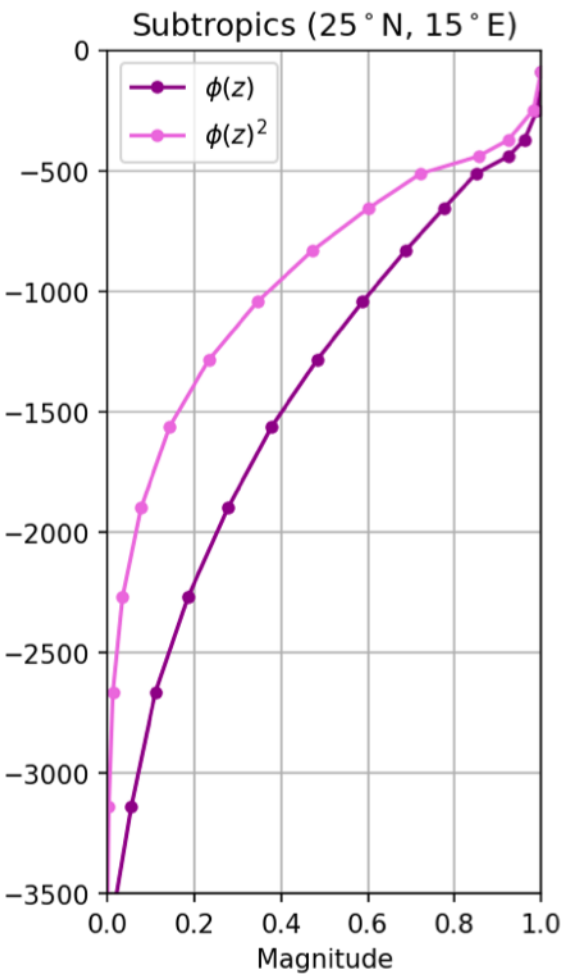
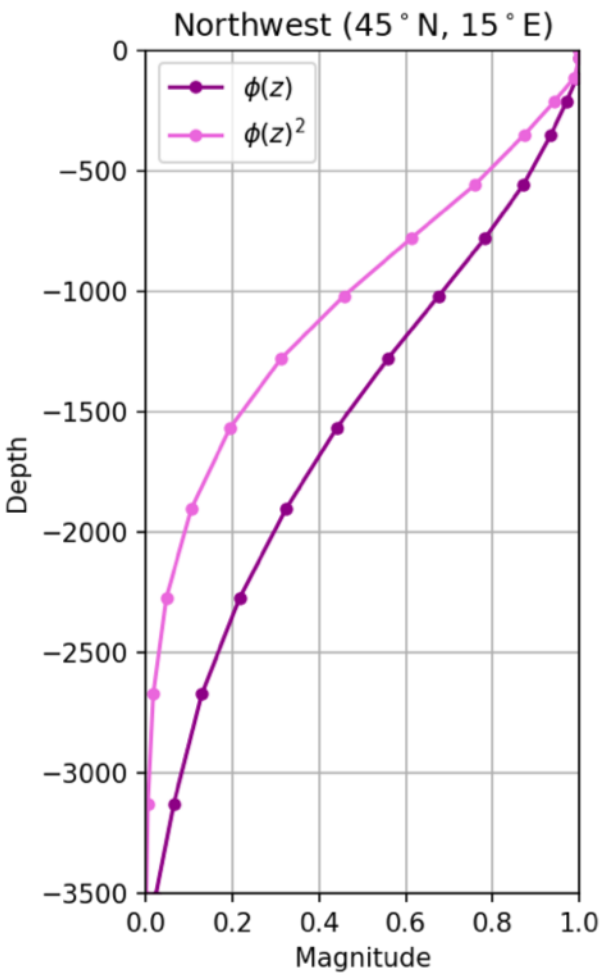


Figure 11.

Backscatter to  
resolved flow ( $\dot{e}_{\text{Bscat}}$ )  
increases



Subgrid eddy kinetic  
energy grows  $\partial_t e > 0$

$$\partial_t e \approx \dot{e}_{\text{Smag}} - \dot{e}_{\text{Bscat}}$$

$$\frac{D\mathbf{u}}{Dt} + f \wedge \mathbf{u} = -\frac{\nabla p}{\rho} + \mathbf{g} - \nu_4 \nabla^4 \mathbf{u} + \nu_2 \nabla^2 \mathbf{u}$$

Resolved velocity  
gradients & kinetic  
energy grow



Resolved viscous  
dissipation ( $\dot{e}_{\text{Smag}}$ )  
increases

Figure 1.

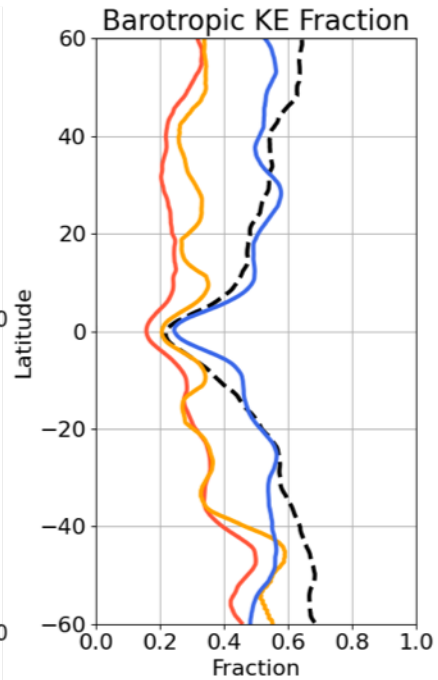
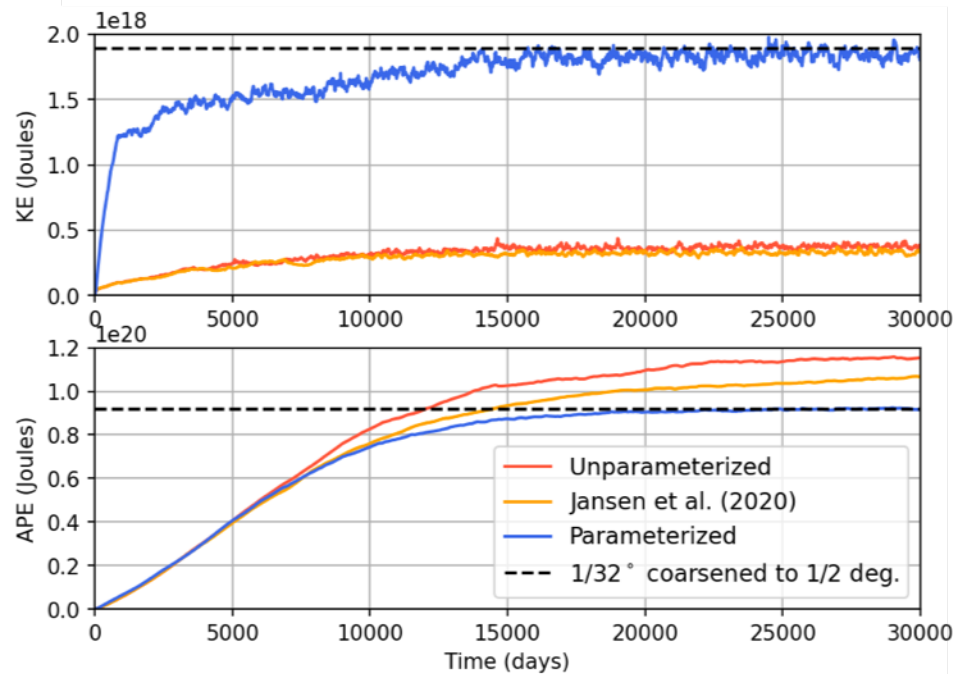
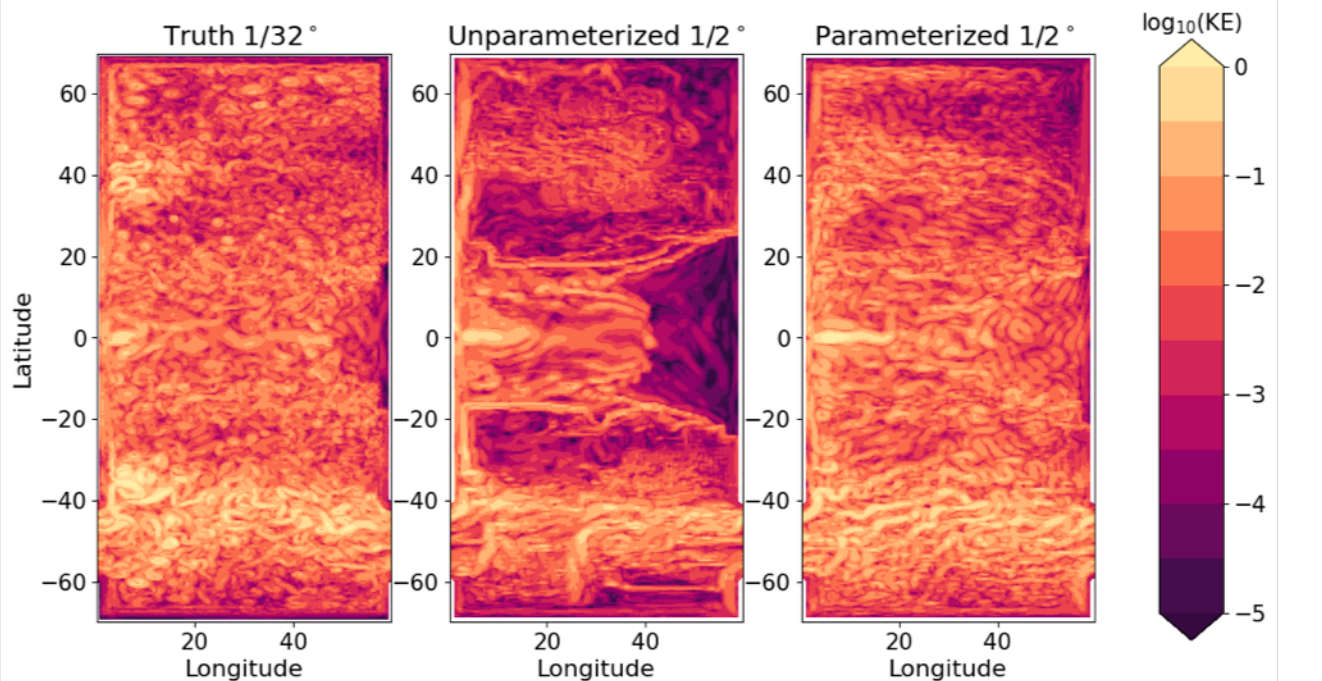
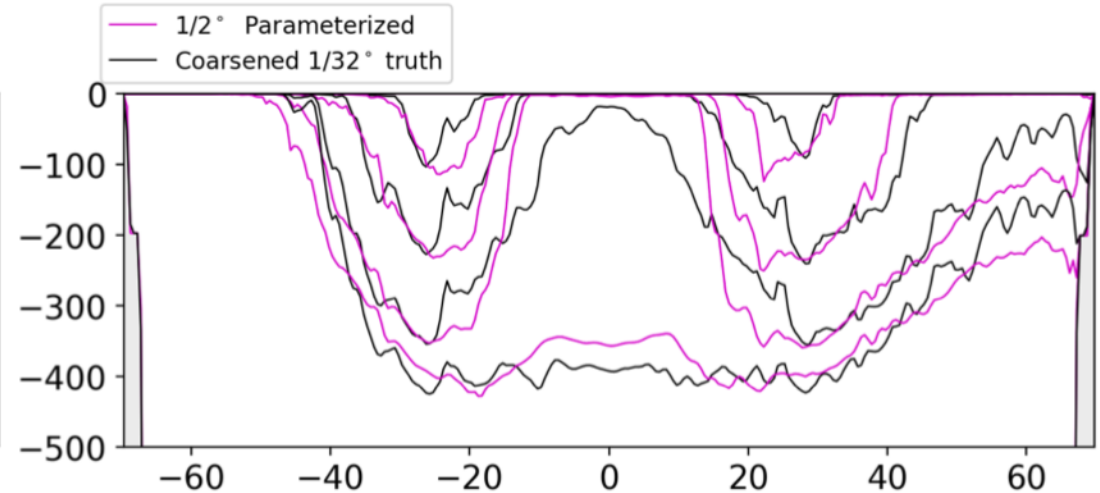
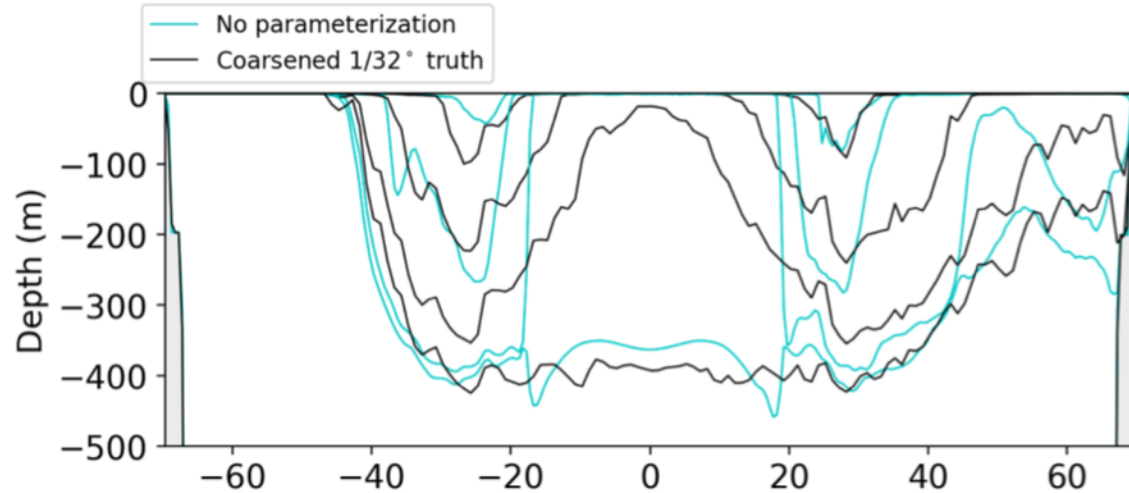
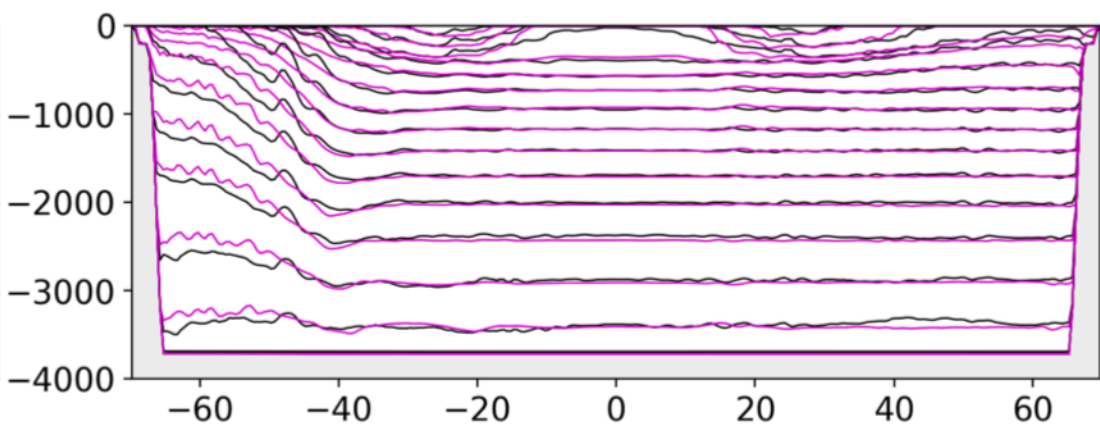
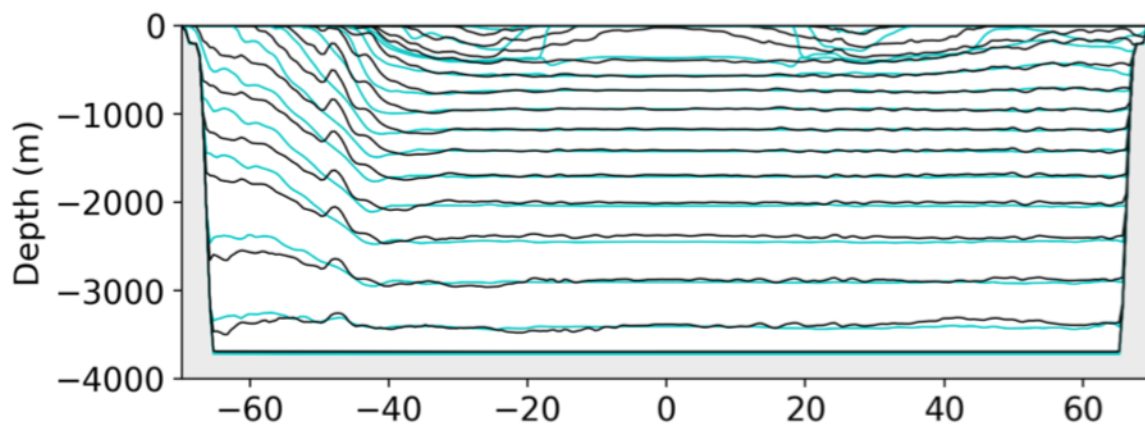


Figure 4.

# Near-Surface



# Full Transect



# ACC Region

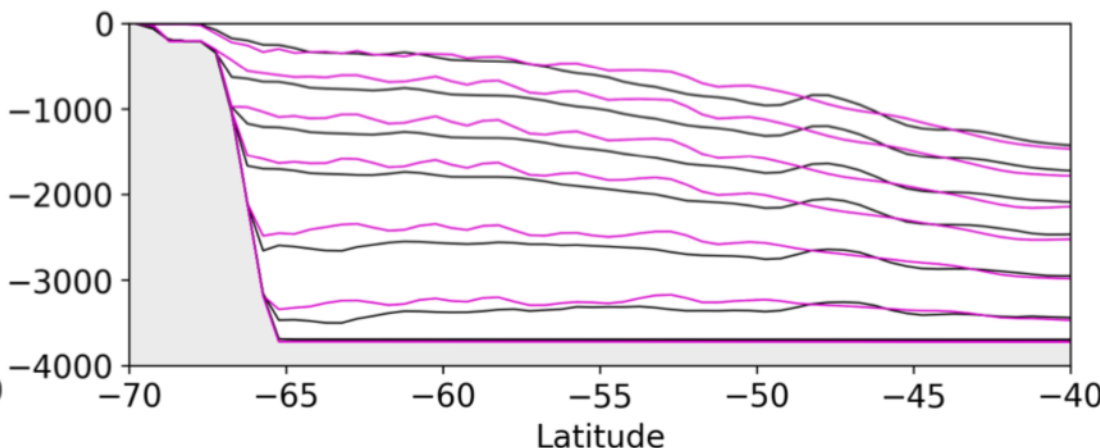
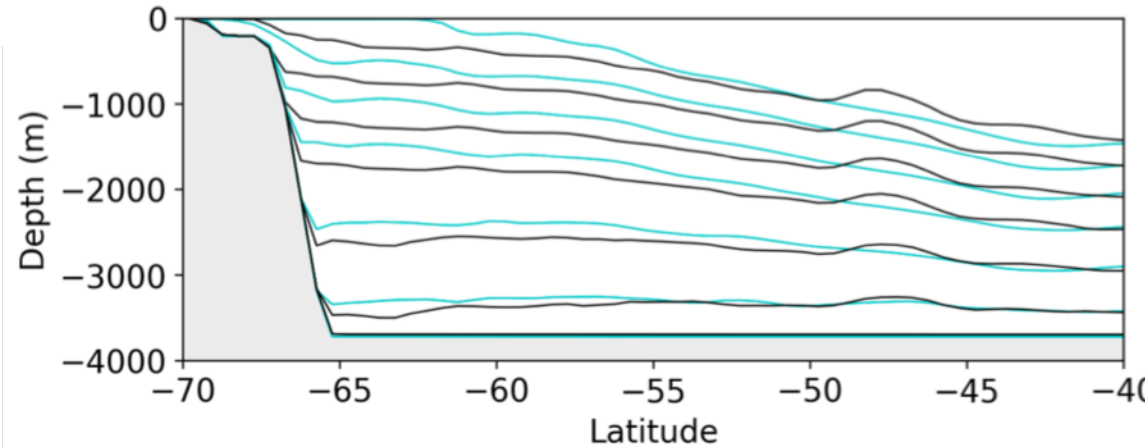


Figure 9.

GM only 1/2 °

Backscatter only 1/2 °

GM+Backscatter 1/2 ° [1/s]

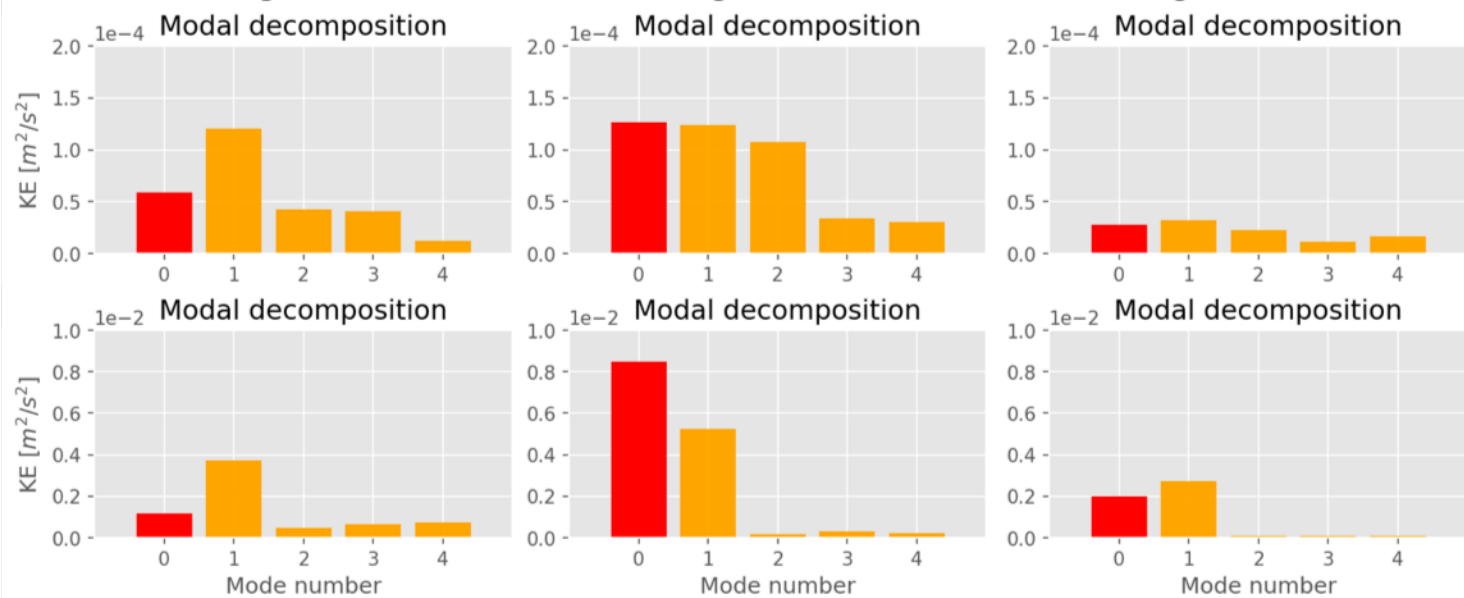
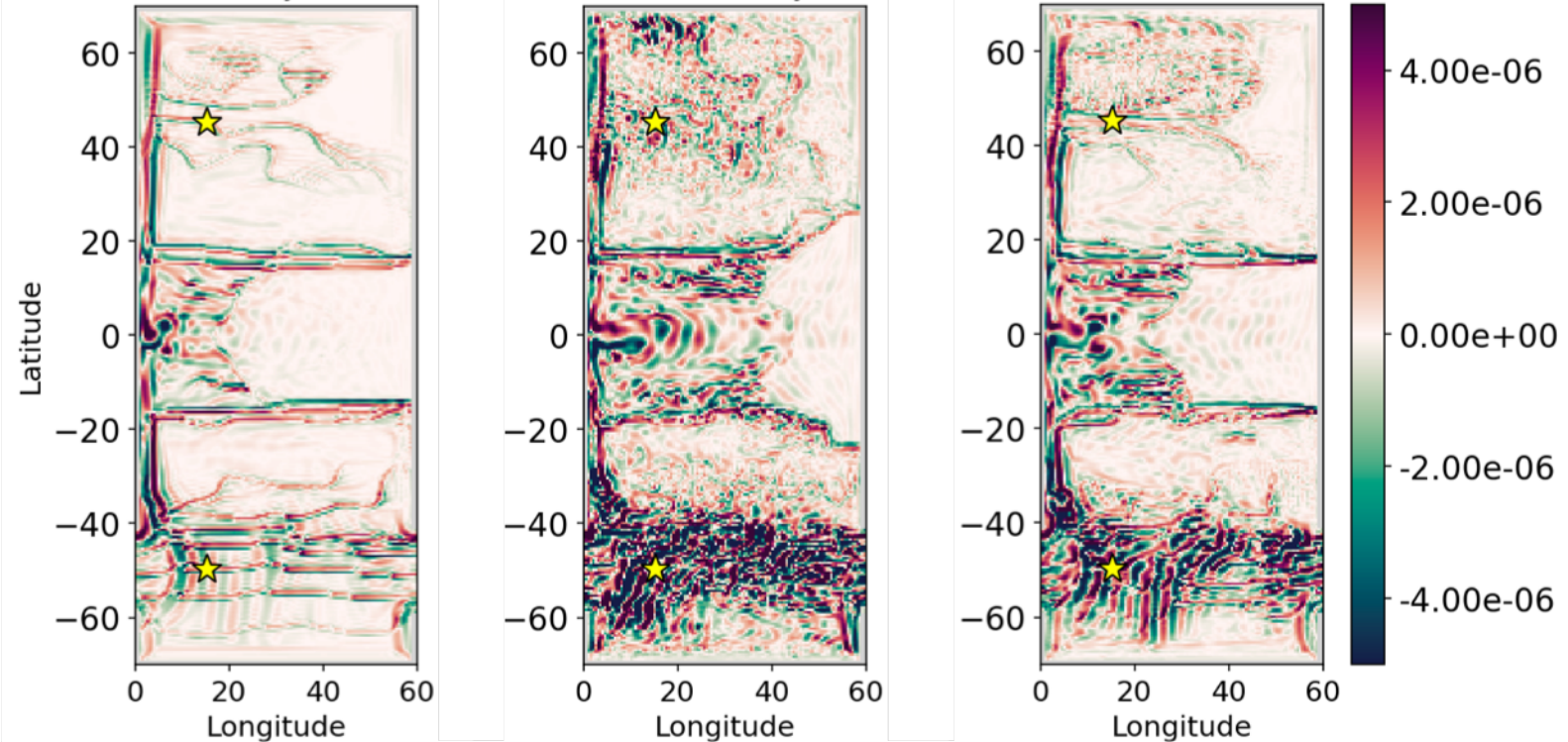


Figure 7.

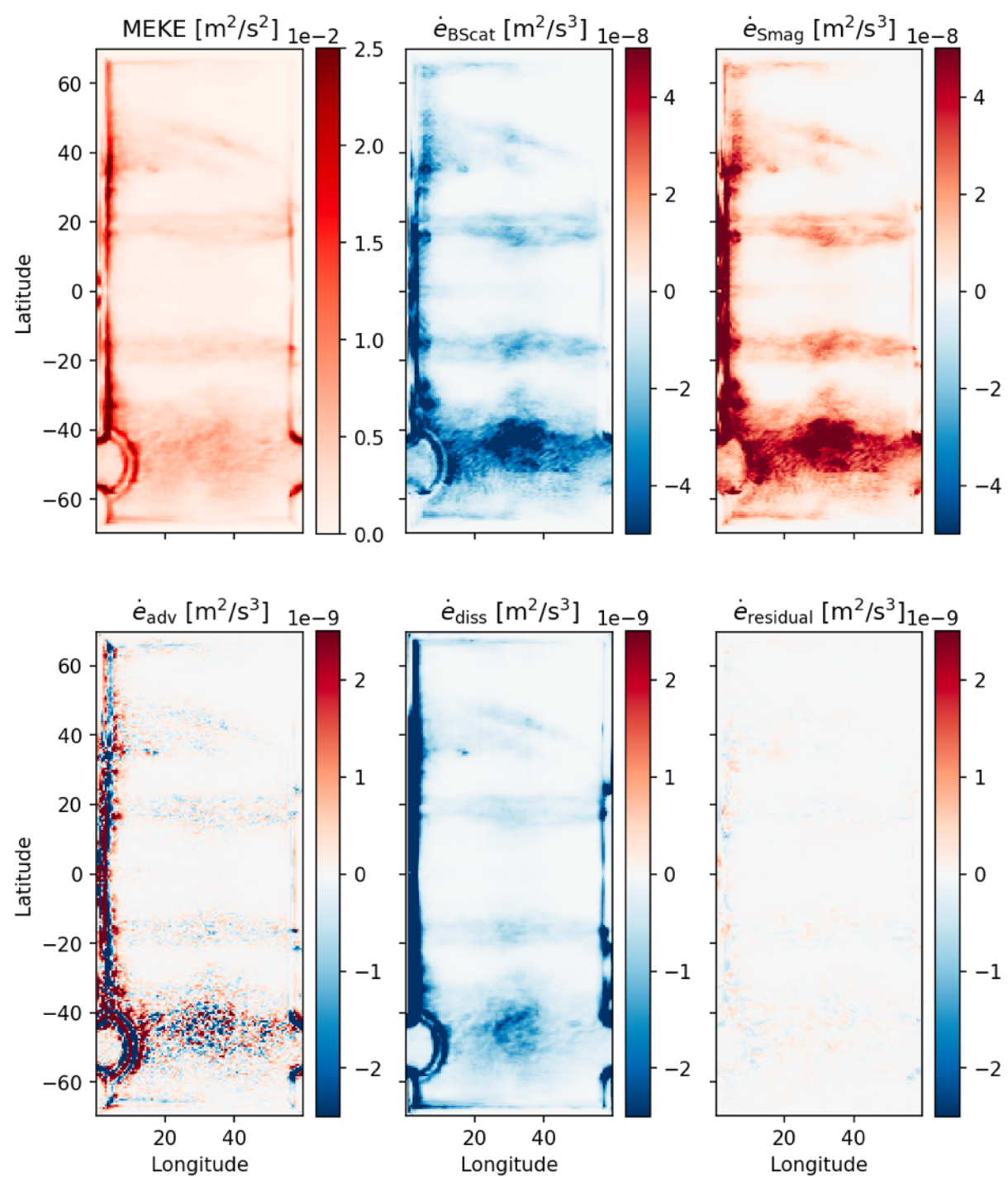
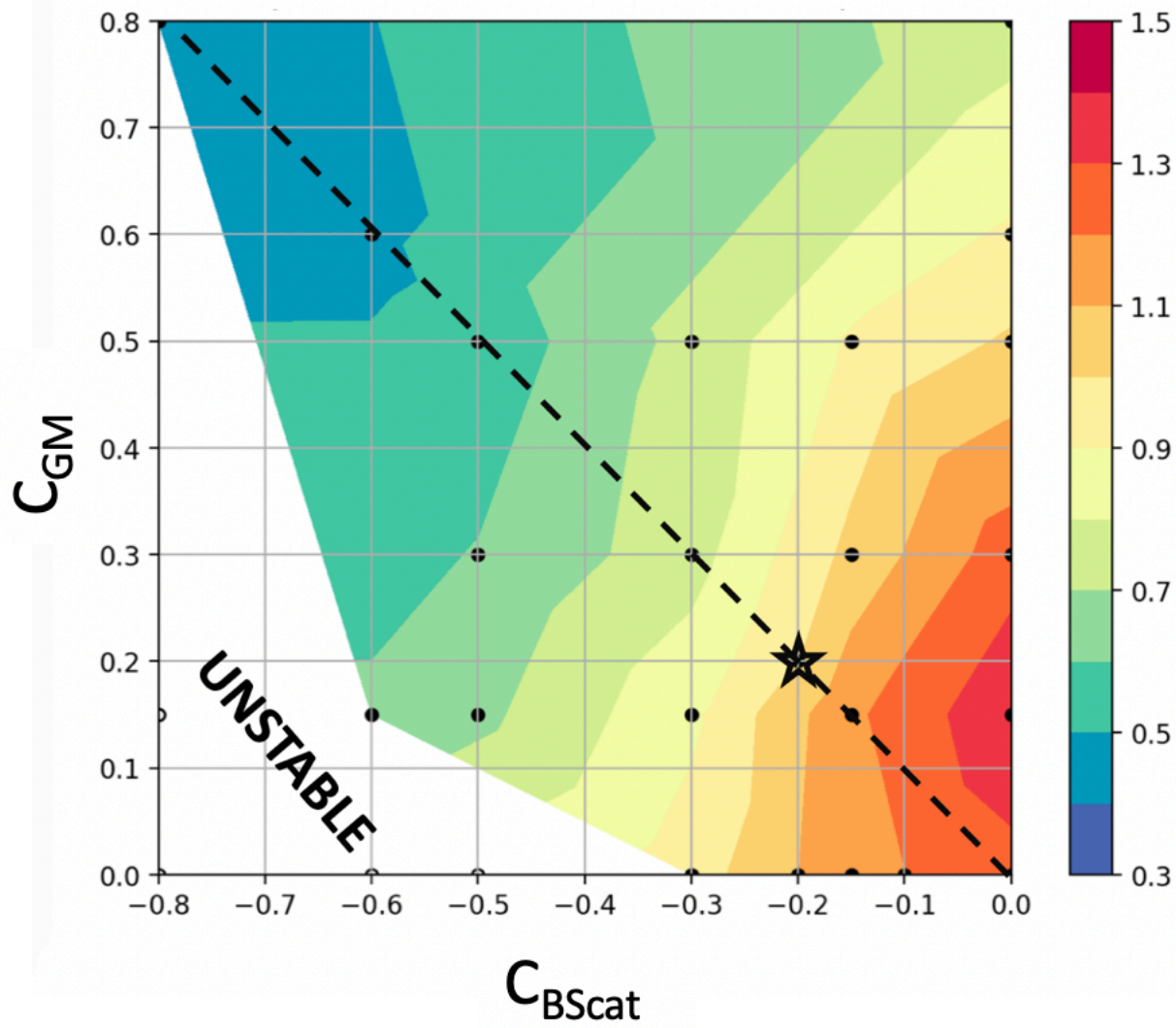
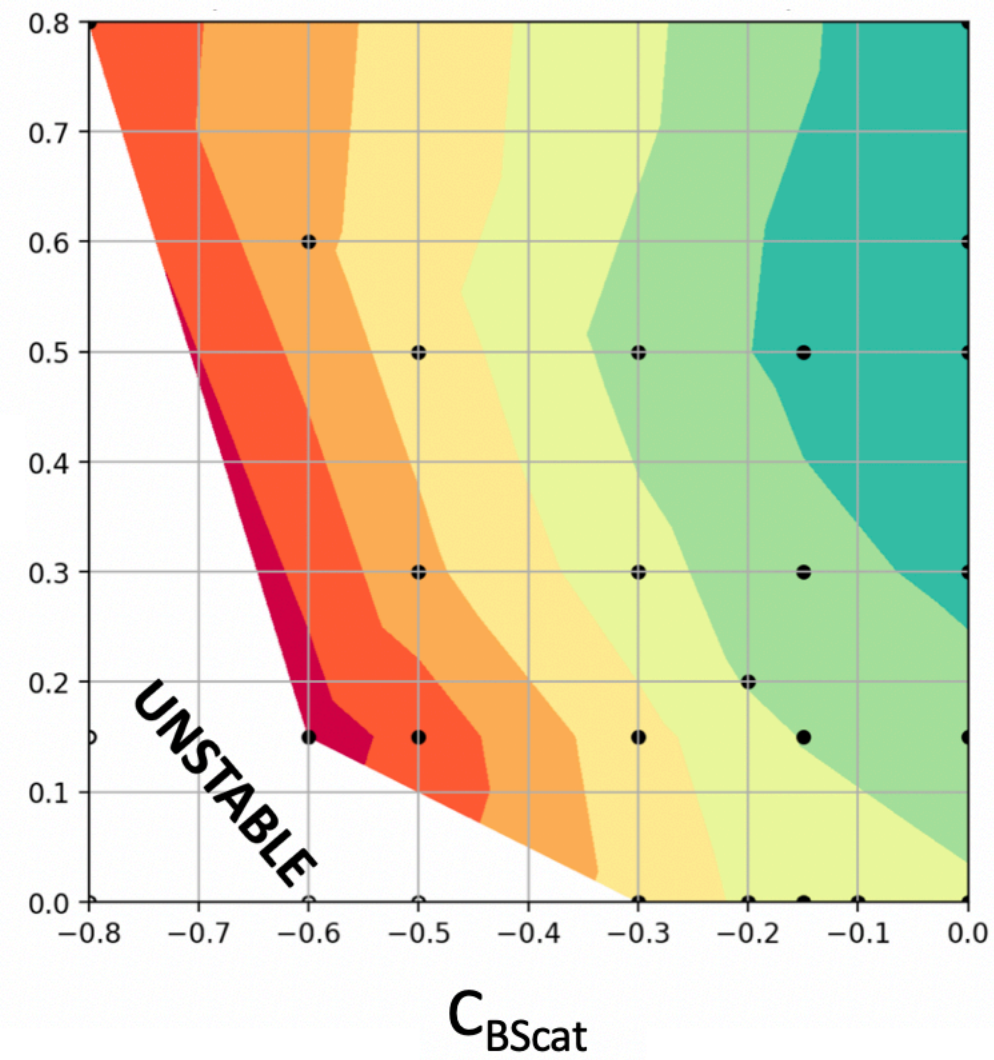


Figure 10.

APE relative to truth



KE relative to truth



BT KE fraction relative to truth

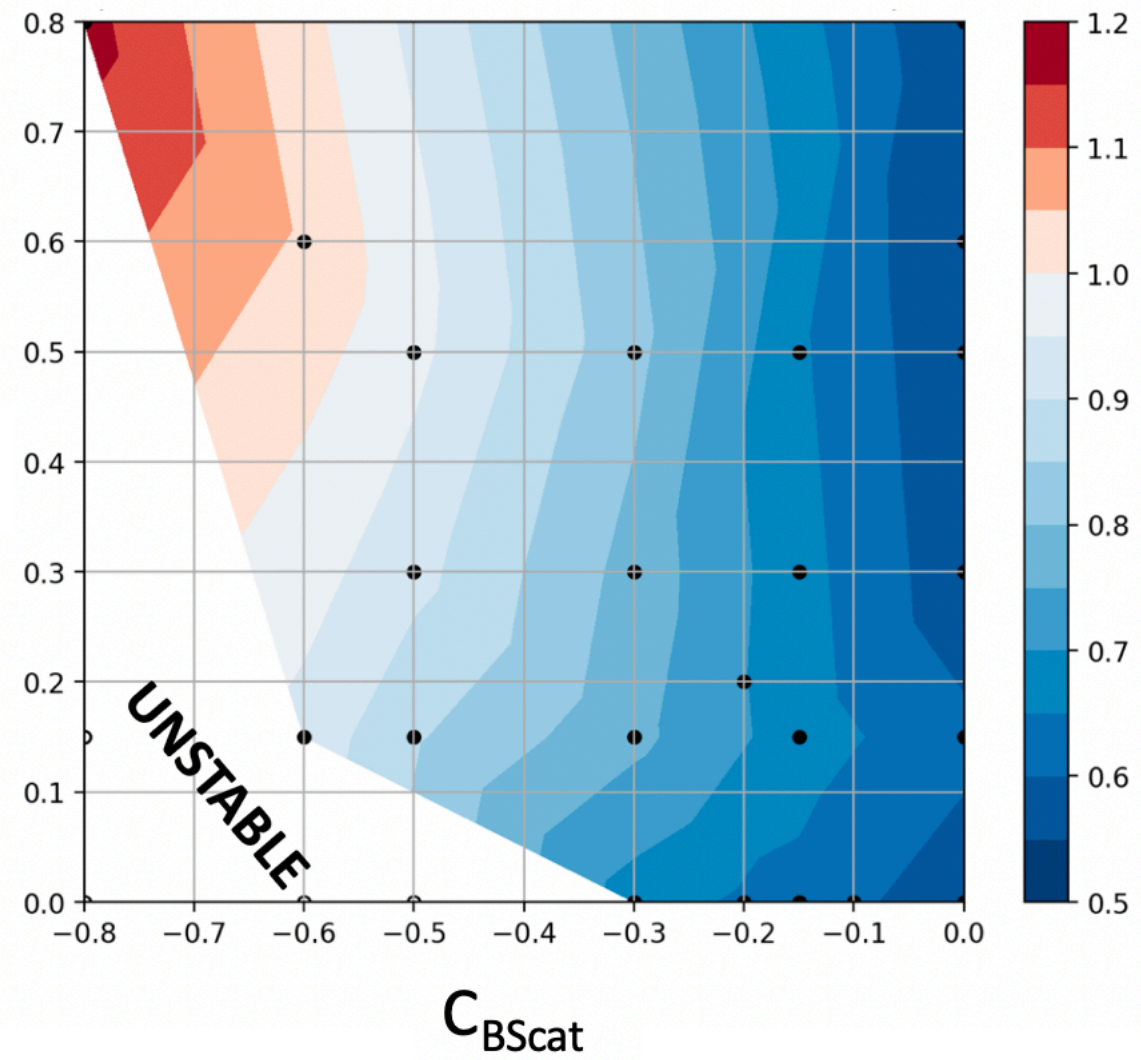


Figure 8.

# Energy Containing Scale Comparison

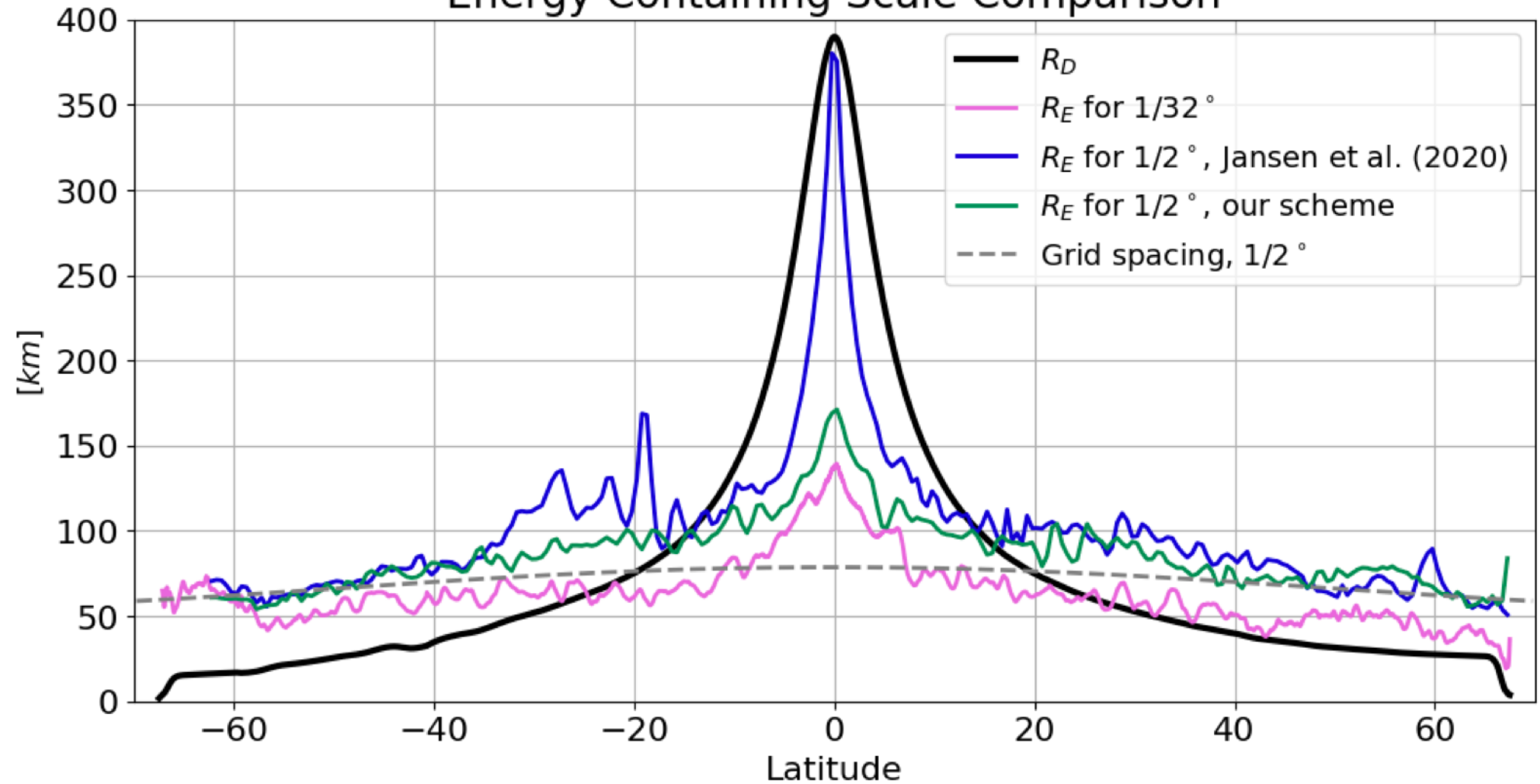


Figure 3.

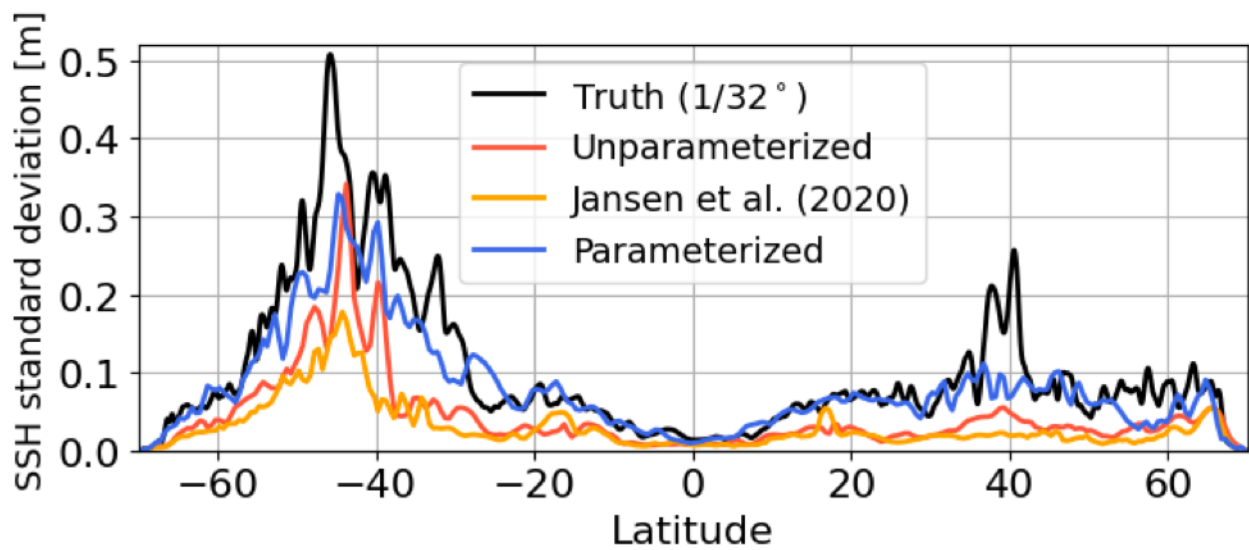
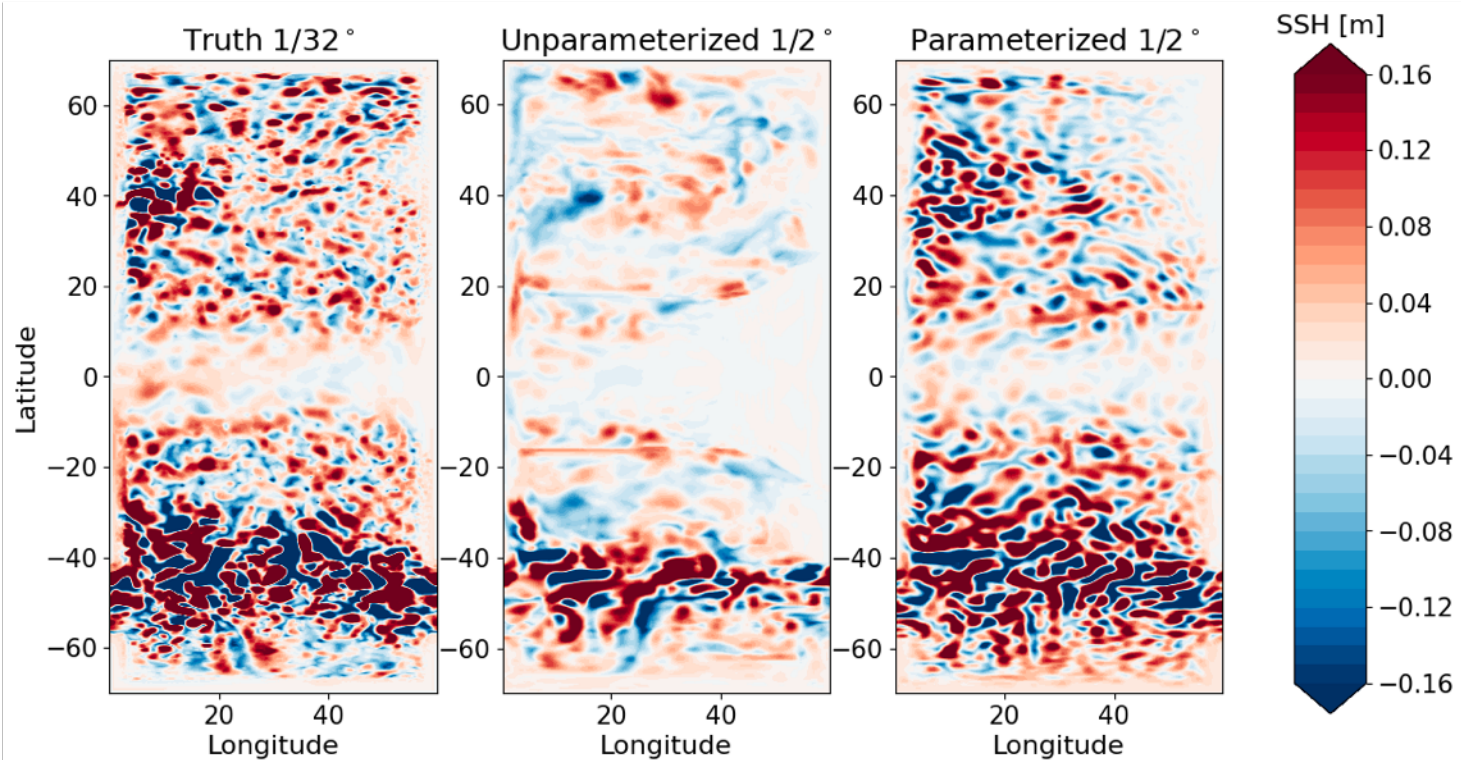
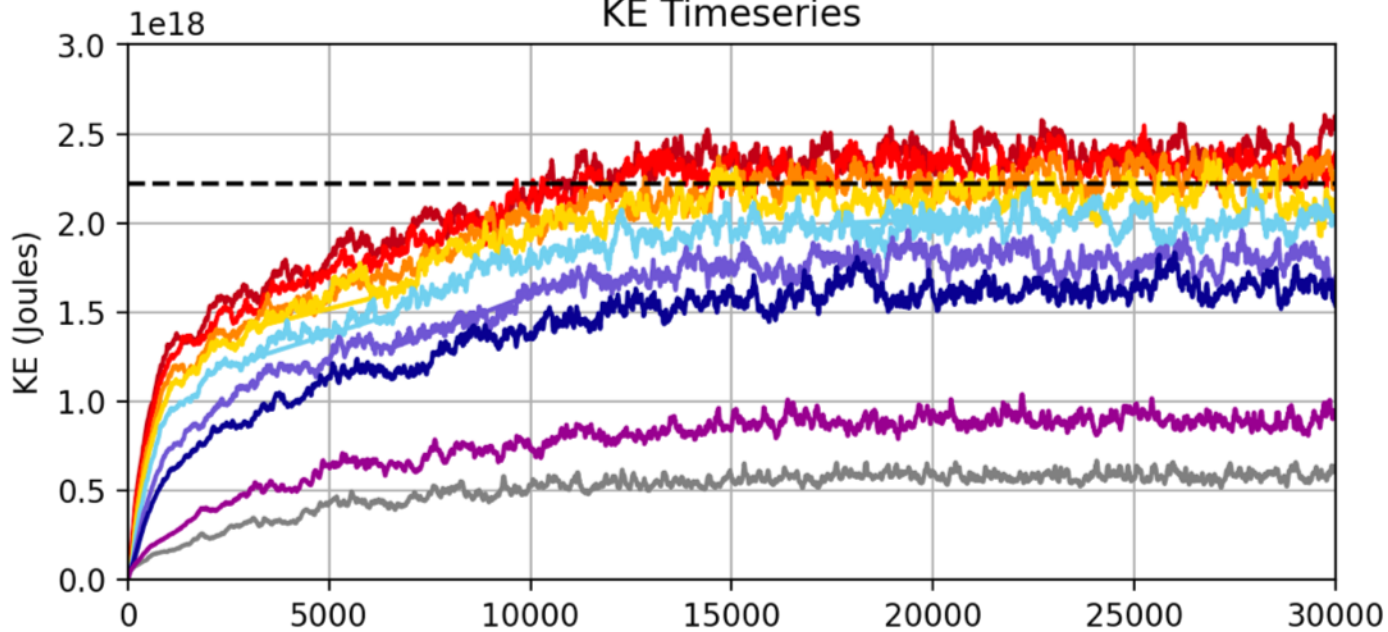


Figure 13.

KE Timeseries



APE Timeseries

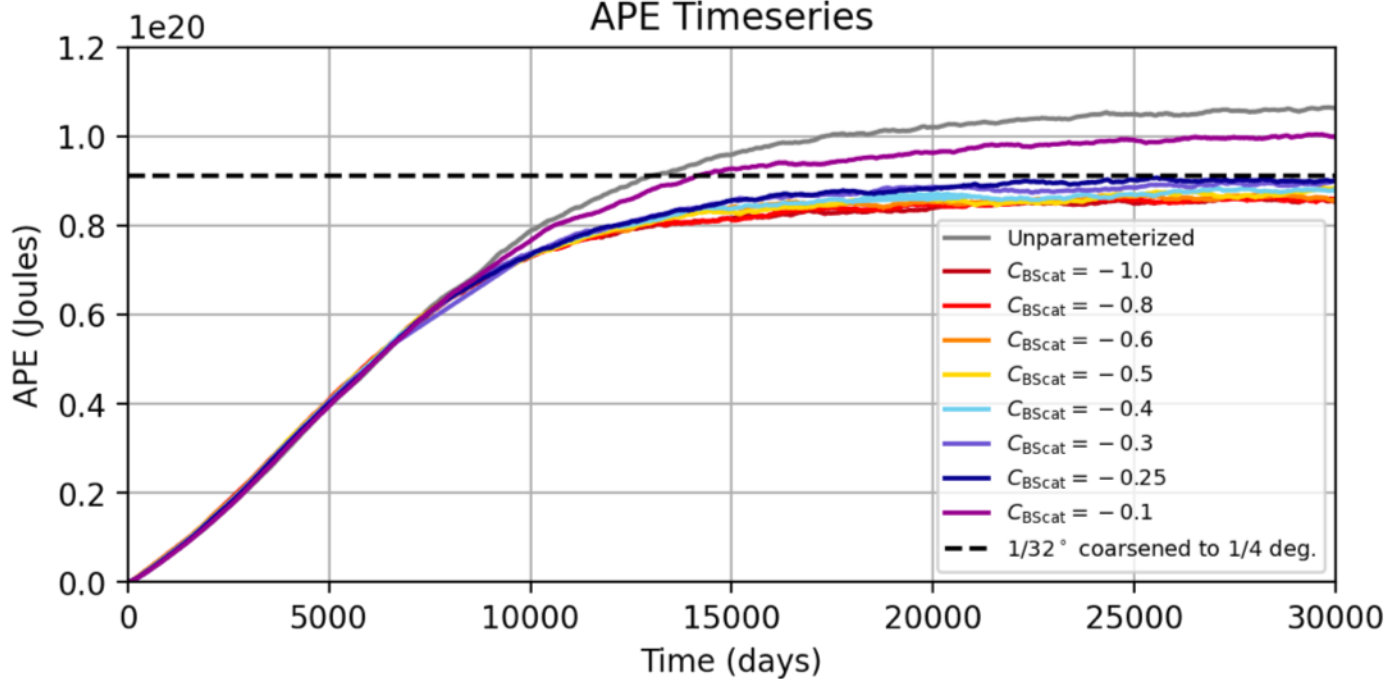


Figure 12.

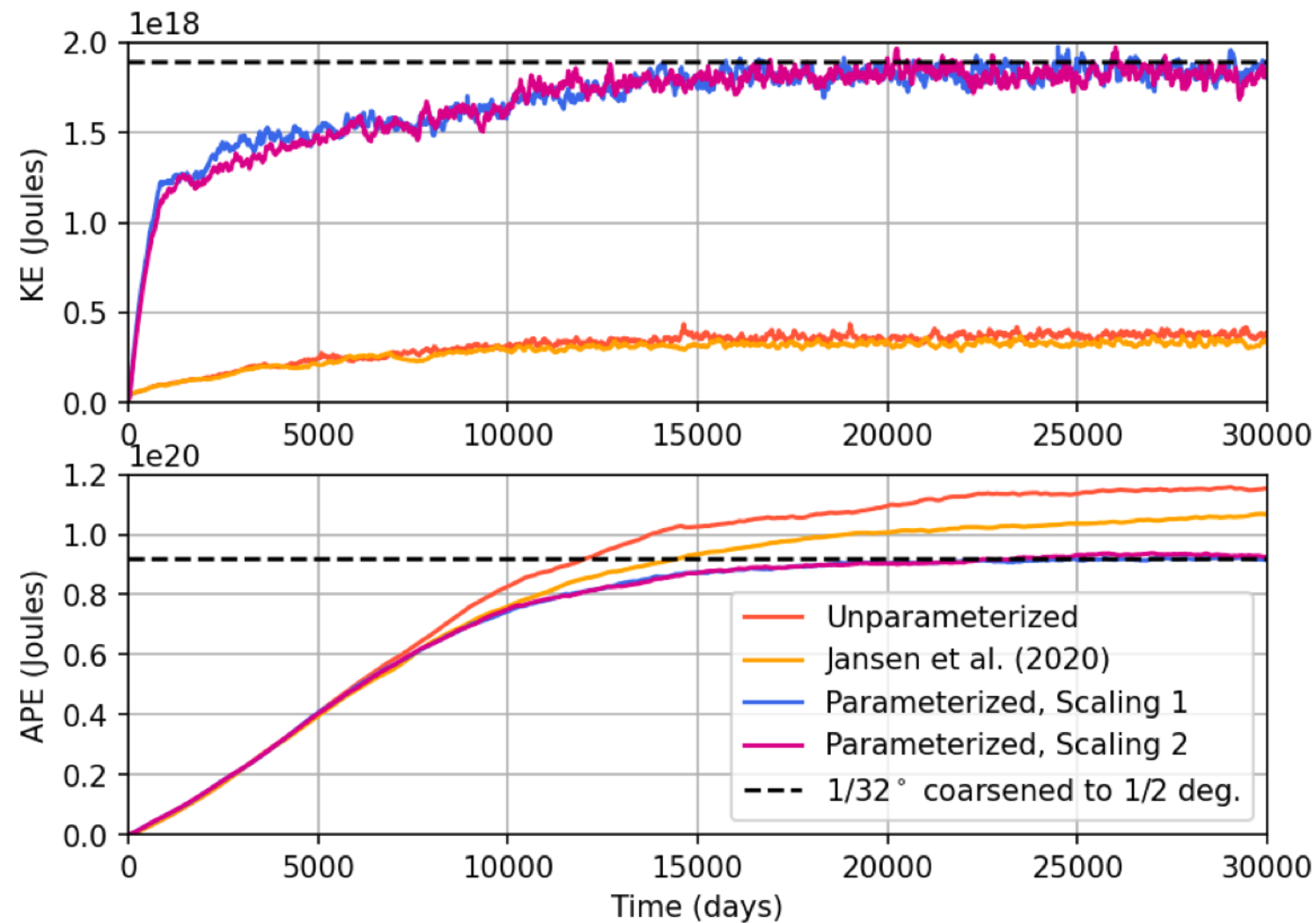


Figure 6.

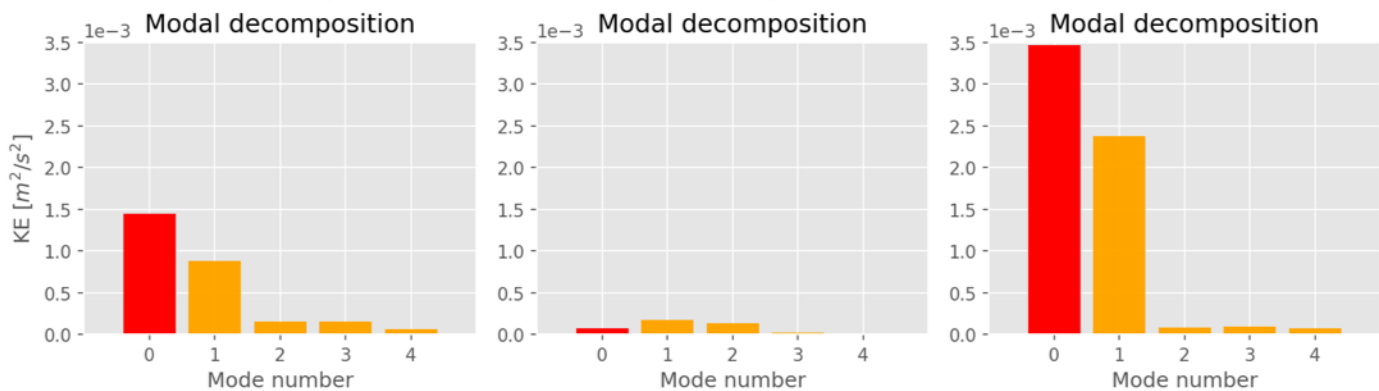
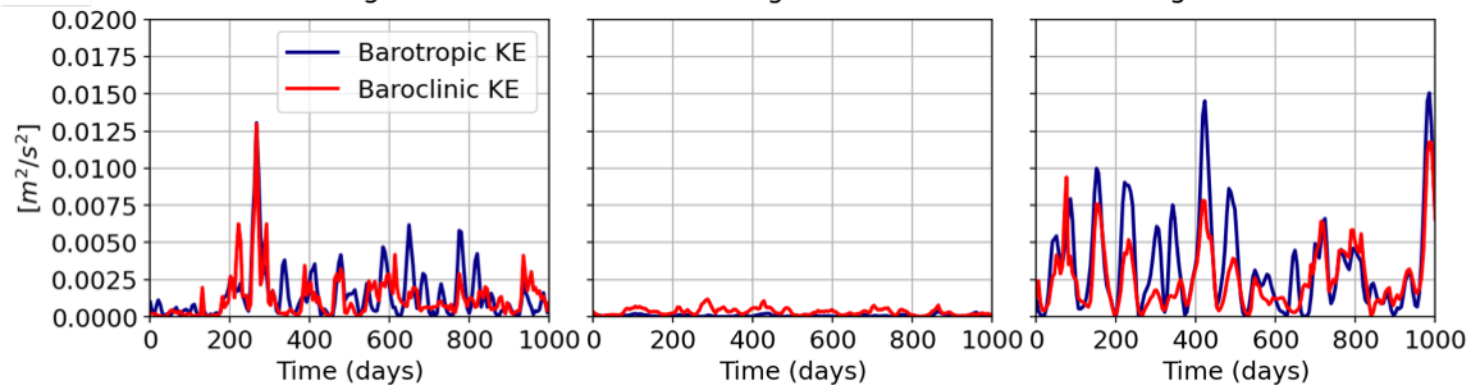
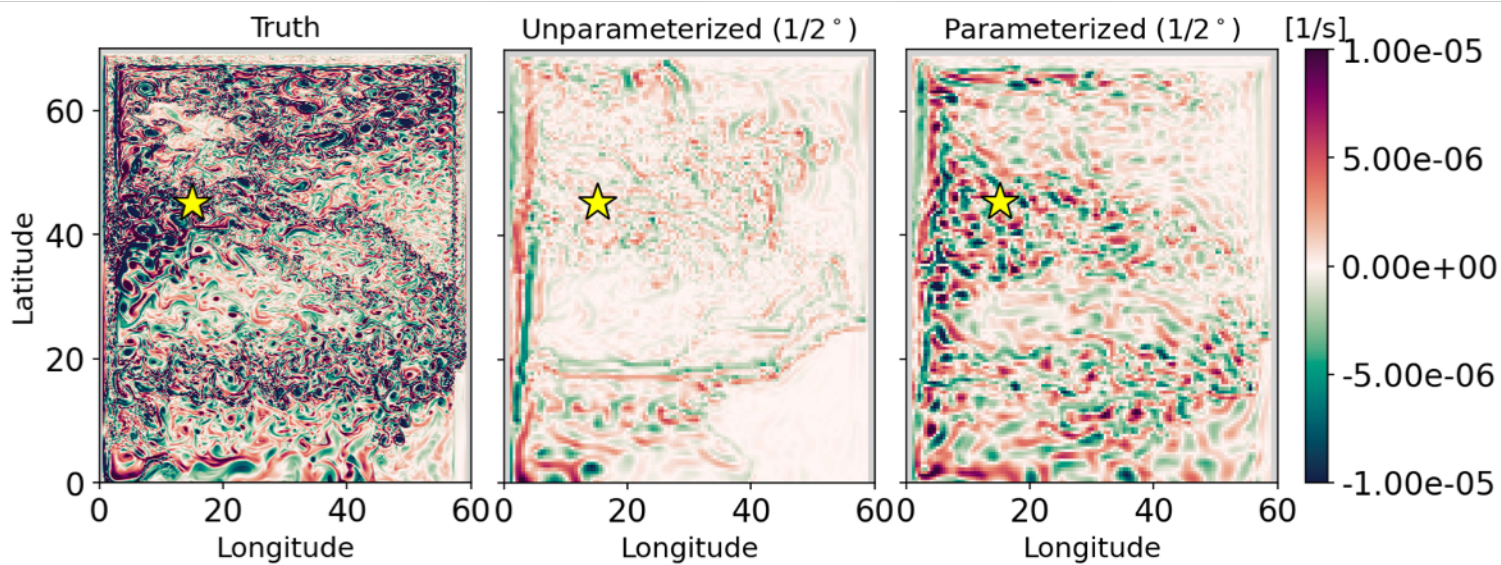


Figure 5.

